

ANALYSIS OF NONEQUILIBRIUM STEADY-STATES

A DISSERTATION SUBMITTED TO
THE GRADUATE SCHOOL OF ENGINEERING AND SCIENCE
OF BILKENT UNIVERSITY
IN PARTIAL FULFILLMENT OF THE REQUIREMENTS FOR
THE DEGREE OF
DOCTOR OF PHILOSOPHY
IN
PHYSICS

By
Ayşe Ferhan Yeşil
November 2016

ANALYSIS OF NONEQUILIBRIUM STEADY-STATES

By Ayşe Ferhan Yeşil

November 2016

We certify that we have read this dissertation and that in our opinion it is fully adequate, in scope and in quality, as a dissertation for the degree of Doctor of Philosophy.

Mehmet Cemal Yalabık(Advisor)

Bilal Tanatar

Azer Kerimov

Süleyman Şinasi Ellialtıođlu

Ali Ulvi Yilmazer

Approved for the Graduate School of Engineering and Science:

Ezhan Karaşan
Director of the Graduate School

ABSTRACT

ANALYSIS OF NONEQUILIBRIUM STEADY-STATES

Ayşe Ferhan Yeşil

Ph.D. in Physics

Advisor: Mehmet Cemal Yalabık

November 2016

Non-equilibrium is the state of the almost all systems in the universe. Unlike equilibrium systems, they interfere with their surroundings which results in never ceasing fluxes. There is no unified theory to understand these systems, since their complexity have no bounds. However, there is a restricted subset of them, namely a steady state, in which system maintains constant fluxes and its macroscopic observables are not changing in time. Majority of the non-equilibrium problems that the scientific community is interested in comprise systems at steady states or the way such systems relax to steady states, due to their relative ease of analysis.

Steady states of Totally Asymmetric Simple Exclusion Processes (TASEPs) are the main focus of this dissertation. We analyze them through Monte Carlo (MC) simulations. The technique is basically a computational experiment done by utilizing random numbers. Performing a computational experiment is a natural way to study these systems since most of the time they are still too complex to have analytical solutions.

We present MC simulation results of our studies on the response of TASEP steady states to sinusoidal boundary oscillations. Typically over-damped systems, such as TASEPs, give monotonous frequency response to sinusoidal driving. However, there are exceptions to these all which draw significant attention from the community, *e.g.*, stochastic resonance. We report a novel resonance phenomena on over-damped systems. We present our results in two different but related works.

In our first work, we study the motion of shock profiles of TASEP with single class of particles under oscillatory boundary conditions using MC analysis. We also model its dynamics as a Fokker-Planck (FP) system, which incorporates a retarded-oscillatory force with a static single well potential. We solve the FP system by numerical integration. We showed that amplitudes of statistical quantities in both of these systems, (*e.g.*, average position), display resonant effects and their results are qualitatively very similar.

In our second work, we showed that by periodically manipulating the boundary conditions of TASEP with two classes of particles, we can achieve otherwise unreachable states of the system by the same parameters. We also report the hysteresis behavior in the same system, existence of which leads to the identification of typical velocity of the system. All these phenomena are the results of resonant response of the particle number density of the system.

Keywords: Non-equilibrium systems, steady states, ASEP, Fokker-Planck Equation, Resonance, Over-damped systems.

ÖZET

DENGEDE OLMAYAN DURUĞAN DURUMLARIN ANALİZİ

Ayşe Ferhan Yeşil

Fizik, Doktora

Tez Danışmanı: Mehmet Cemal Yalabık

Kasım 2016

Doğadaki hemen her sistem dengede olmayan sistemdir. Dengede olan sistemlerin aksine, bu sistemler daimi bir madde veya enerji akışı oluşturacak şekilde çevreleriyle etkileşirler. Karmaşıklıklarının bir üst sınırı olmadığından hepsini bir çatı altında birleştirecek bir teori de yoktur. Bu sistemlerin karmaşıklığının daha kısıtlanmış bir hali olan durağan durumlarda ise sistemdeki akış sabittir ve sistemin gözle görülebilen özellikleri zaman içinde değişmez. Analiz etmenin kolaylığı nedeniyle, araştırmacıların ilgilendiği dengede olmayan sistemler çoğunlukla ya durağan durumdadır ya da durağan duruma gelmeye çalışmaktadır.

Tezimin merkezinde durağan durumdaki tamamen asimetric basit dışlama süreçleri (TASEP) var. Bu sistemleri biz Monte Carlo simülasyonları ile analiz ettik. Bu teknik temel olarak rastgele sayıları kullanarak yapılan bilgisayar deneyidir. Çoğu zaman bu sistemler analitik olarak çözülebilmek için çok karmaşık olduğundan onları bilgisayarlı deneyler yaparak anlamaya çalışmak sıklıkla kullanılan bir yöntemdir.

Biz TASEP durağan durumunun sinüs biçimli sınır koşullarına olan tepkisinin MC simülasyonu ile elde edilen sonuçlarını sunuyoruz. Alışla geldik haliyle frekans bakımından TASEP gibi aşırı-sönümlü sistemlerin sinüs şeklindeki sürülmelere tepkisi tekdüzedir. Ama bunun dışında kalan olasılıksal (stokastik) rezonans gibi bilim insanların ilgisini oldukça fazla çekmiş örnekler de bulunur. Biz de aşırı sönümlü sistemlerde yeni bir rezonans olgusunu bildiriyoruz. Bununla ilgili sonuçlarımızı birbirinden farklı ama birbirleriyle alakalı iki iş halinde sunacağız.

İlk işimizde tek tür parçacık bulunduran TASEP sistemine ait şok yapılarının sinüslü yapıda sınır koşulları altındaki hareketini MC yöntemiyle analiz ettik. Aynı zamanda bu sistemin dinamiklerini bir tek çukurlu durgun potansiyeli ve bir de rötarlı sinüs yapıda kuvveti olan aşırı-sönümlü Fokker-Planck (FP) sistemi olarak da modelledik. Bu FP sistemini nümerik integral alma yoluyla çözdük.

Gösterdik ki iki sistemde de bulunan ortalama konum gibi kimi istatistiksel nicelikler rezonans özellikleri sergilemekte ve iki sistemin sonuçları birbirlerine oldukça benzemektedir.

İkinci işimizde ise iki türde parçacık bulunduran TASEP sisteminin sınır koşullarına periyodik şekilde müdahale ederek aynı değişkenlerle başka türlü elde edemeyeceğimiz durumlara ulaşabilmenin mümkün olduğunu gösterdik. Aynı sistemin histeresis davranışı, ki sayesinde sistemin kendine özgü hızını tespit edebildiğimiz davranıştır bu, gösterdiğini bildirdik. Tüm bu bahsi geçen olgular sistemin içindeki parçacık sayısının rezonans davranışı sergilemesinin sonucu olarak ortaya çıktı.

Anahtar sözcükler: Dengede olmayan sistemler, durağan durum, ASEP, Fokker-Planck Denklemi, Rezonans, Aşırı Sönümlü Sistemler.

Acknowledgement

To my beloved family, my dearest friends, my boyfriend and especially to my mother.

I am indebted to my advisor for his patience, care and endless motivation of sharing his knowledge with me. And I am also indebted to Department of Physics for their support during my PhD.

Contents

1	Fundamentals	1
1.1	Introduction	1
1.2	Equilibrium Statistical Mechanics	4
1.2.1	Phase Transitions	4
1.3	Non-equilibrium Statistical Mechanics	9
1.3.1	Near-Equilibrium Systems	9
1.3.2	Aging Systems	10
1.3.3	Far from Equilibrium Systems	11
1.3.4	Steady States	11
1.3.5	Phase Transitions	12
1.4	The Model: Asymmetric Simple Exclusion Process	15
1.4.1	Definitions and general properties	15
1.4.2	Universality class, hydrodynamic limit and mappings of ASEP	19
1.4.3	Exact Solutions	26
1.4.4	Applications	27
2	First order phase transitions: Shock profiles	30
2.1	Single Class of Particles	31
2.1.1	Phase Diagram	32
2.1.2	Shock Profile	33
2.2	Two Classes of Particles	36
2.2.1	Phase Diagram	38
2.2.2	Shock Profile	40

3	Methodology	43
3.1	Master Equation	43
3.2	Monte Carlo Analysis	45
3.3	Kinetic Monte Carlo	47
3.4	Fokker-Planck Equation	48
4	Original Work	52
4.1	Strong Frequency Dependence in Over-damped Systems	52
4.1.1	Analysis and Discussions	55
4.2	Dynamical Phase Transitions in TASEP	68
4.2.1	TASEP under Periodically Driven BC	70
4.2.2	Variations in the character of Frequency Dependence	70
4.2.3	Pulse Response	80
5	Conclusions	85

List of Figures

1.1	Detailed balance (a) vs steady state (b). Even though in both of the cases probability of A,B,C are all equal (when all ω 's are equal) and one third, in the steady state there is always a probability current in the clockwise direction. So steady state is a weaker condition than the detailed balance and it carries the condition of non-equilibrium systems, that is, non-vanishing currents.	3
1.2	These are common schematic diagrams of free energy for first and second order phase transitions. Each well in the free energy corresponds to an ordered state. T_t corresponds to the tuning parameter of the transition, and T_c corresponds to the critical tuning parameter. . . .	8
1.3	ASEP dynamics on periodic and open boundary conditions.	16
1.4	Each surface with $-\pi/4$ degree slope maps to occupied site and with $+\pi/4$ degree slope maps to a vacancy. Red lines indicates how hopping of ASEP particles will change the texture of the surface. After the hopping, slope of the occupied site becomes $-\pi/4$, and the vacant site becomes $+\pi/4$	22
1.5	Lattice sites in ZRP mapped to vacancies in ASEP, and particles mapped to adjacent occupied sites on the left of the vacancy their site mapped.	23
2.1	One species, open boundary TASEP model.	31
2.2	Phase diagram of TASEP with single species, with open boundary conditions.	33

2.3 Shock profile for different numbers of particles in a lattice of 50 sites. i indicates the site, $\rho_n(i)$ indicates the density profile that corresponds to the n number of particles. 36

2.4 Schematic description of TASEP with two species of particles under open boundary conditions. 37

2.5 Mean field phase diagram of TASEP with two types of particles. Here $\alpha_1 = \alpha_2 = \alpha$, $\beta_1 = \beta_2 = \beta$ and $\gamma_1 = \gamma_2 = \delta = 1$ 38

2.6 Schematic density vs lattice plot for TASEP with two classes of particles. In the left box the lattice is in TR phase. However on the right box it is in HL phase. It displays that these two phases can coexist. 41

2.7 Schematic density vs lattice plot for TASEP with two classes of particles. First-class particles display the shock profile, for various numbers of particles in the lattice. Whereas, the second-class particles remains in low density state (LD). 42

4.1 First Fourier components that give the magnitude of the oscillatory response (as the expectation value of the position) of the system as a function of wavelength. Each plot corresponds to different values of boundary smoothness x_0/L . Dotted line corresponds to the cosine (C) or out of phase component and continuous line corresponds to the sine (S) or in phase component. Notice here that the scales of the plots are not equal. 57

4.2 The probability densities of marked points in Fig. 4.1. (a) Point **A** ($\lambda = 0.6$) accounts to consecutive dark and light patterns along the x-axis, which indicates standing waves of two wavelengths that fits to the lattice size. (b) Point **B** ($\lambda = 1.6$) accounts to only one wavelength. 58

4.3 Shock profile distributions for various numbers of particle number. 60

4.4 The linear relationships between particle number n and shock position x_s for the profiles in Fig. 4.3. The shock position x_s is defined as the lattice position at which the density $\rho_n(i)$ corresponds to the midpoint of the profile. The inset displays the relationship when boundary conditions change sinusoidally with period τ as discussed in the text. Here $N = 50$ and $\tau = 120$ 62

4.5 Probability distribution $P(n)$ of particle number n ., for a lattice size of $N = 50$ and $\alpha = \beta = 0.1$ 63

4.6 Response of the probability distribution function $P(n)$ to a pulse type perturbation to the entrance rate. The arrows shows the maxima of the curves. See text for the details. 64

4.7 Change in probability density $\rho(n, t)$ from its time average. Point a and b are marked in Fig. 4.2. (a) Point a ($\tau = 140$) accounts to two wavelengths. (b) Point b ($\tau = 700$) accounts to one wavelength of the system. Simulations are carried out for $N = 50$ and different periods calculated over 10^6 MCS. 67

4.8 Fundamental components (C and S in Eqn. 4.8) with respect to different period values. It is apparent that the response of the system has resonance like structure. Points **a** and **b** correspond to the density distributions in FIG. 4.7. Inset shows there is also sinusoidal behavior present for smaller values of τ 67

4.9 Joint probability density functions $p(n_1, n_2)$ for various paramaters under constant BC. Exit rates for the plot (a) are $\beta_1 = \beta_2 = 0.285$, for the plot (b) are $\beta_1 = \beta_2 = 0.275$, and for the plot (c) are $\beta_1 = \beta_2 = 0.265$, and for the plot (d) they are asymmetric as $\beta_1 = 0.265$ and $\beta_2 = 0.285$. For all of the graphs the rest of the rates are equal to 1. 68

4.10 Various shock profiles in a system size of $N = 100$. Time-independent boundary rates are $\alpha_1 = \alpha_2 = 1$ and $\beta = 0.2675$ 69

4.11 Time dependence of the joint density distribution $\rho(n_1, n_2)$ corresponding to the marked points in Fig. 4.12. In each plot, the density at time t as well as density at $t + \tau/4$ (dashed lines) are drawn together to display the motion or the change of shape. Here $N = 200$ and $\Delta\beta = 0.1$ 74

4.12 Average density spread ($\bar{\Delta}$) graph with respect to different period values. Inset shows the average spread for higher values of period. Interesting points are labeled with letters (see details in text). Density distribution for these points are given in Fig. 4.11. 75

4.13 Average density spread ($\bar{\Delta}$) responses of the system for different magnitudes of perturbation, $\Delta\beta \in 0.05, 0.1$. It is apparent that the extrema of the response is independent of the size of the periodic drive. 76

4.14	Average density spread ($\bar{\Delta}$) with respect to oscillation period τ for various values of lattice sizes. Both axes are scaled by N	77
4.15	Hysteresis plots as a function of different periods of oscillation (τ). They are formed by following the trajectory of $\langle n_2 \rangle_{t_i}$ vs $\langle n_1 \rangle_{t_i}$ for values of t_i within a period. The trajectory reaches its limiting forms (two of them are present) starting from $\tau \geq 5000$ and below $\tau \leq 500$	78
4.16	Hysteresis area for two different perturbation magnitudes, $\Delta\beta = 0.05$ and $\Delta\beta = 0.1$ and $N = 200$. The inset shows close up to the phase transition point.	79
4.17	$P(n_1, t)$ for various values of t . $P(n_1, 10000)$ is a near steady-state distribution.	81
4.18	Shock densities corresponding to $n_1 = 30$ for various values of t	82
4.19	Shock profiles that are associated to particle number $n_1 = 65$ for various times t elapsed after the pulse.	83
4.20	Relaxation of the deviation $\delta_1(t)$ for smaller and larger values of n_1 for $N = 100$. Inset shows $\delta_1(t)$ for all values of n_1	84

List of Tables

2.1	Density and current values that correspond to the phases of TASEP.	32
4.1	Dimensionless quantities that are used in scaling the Fokker-Planck equation.	59

Chapter 1

Fundamentals

1.1 Introduction

Better part of the phenomena of nature is at non-equilibrium state. That is, one way or another they are subject to change in time. Some of them are changing as slow as the lifetime of the universe while others are changing as fast as the neutralization reaction of an acid and a base. Besides if not at the time being, things will eventually change by being subject to flux of energy or matter or both, to or from their surroundings. These vast non-equilibrium phenomena has yet to be explained by a general theory. However, whether such a general theory exists itself is subject to discussion. Once, this problem is addressed by John von Neumann as “the theory of non-elephants,” [1] by which, as Per Bak claimed, he meant there may not be any such theory since the subject matter is overwhelmingly diverse.

Nonetheless, systems at far from equilibrium have to be studied in some way, with or without a general theory. One of the most common approaches to study a non-equilibrium system is to construct a simple model. Of particular interest are the models that demonstrate the curious phenomena of non-equilibrium

systems with simple dynamical rules. Totally asymmetric simple exclusion processes (TASEP) are considered as one of those; they are generally accepted as the paradigmatic model for non-equilibrium systems (NES) [2].

In contrast, there is a well-established general theory for equilibrium systems. This accomplishment is due to the very powerful condition called **detailed balance** (see Fig.1.1). Namely, each transition between the micro-states (a macroscopic state is composed of micro-states) should be equilibrated by its reverse transition. Mathematical expression for this condition can be expressed as

$$P_i \omega_{i \rightarrow j} = P_j \omega_{j \rightarrow i}, \quad (1.1)$$

where P_i is probability of state i , $\omega_{i \rightarrow j}$ is transition rate from state i to j and $i, j \in A, B, C$. Equation 1.1 leads to another powerful condition associated to equilibrium systems, i.e, **time-reversal** symmetry of the system. Both of these properties add up to the **ergodicity condition**: ensemble average (average over all possible copies of the system) and the time averages are equal. Therefore, at equilibrium all micro-states that map to the same macro-state energy E have equal probabilities, which is proposed by Gibbs as being proportional to $e^{-E/k_B T}$ [3].

After excluding systems that satisfy the aforementioned conditions, everything else yields non-equilibrium states. We will study a sub-class of non-equilibrium systems, namely steady states in which flux is constant throughout the system. In particular we will focus on steady state of a one dimensional model system named asymmetric simple exclusion process (ASEP).

Organization of this dissertation thesis is as follows: In this chapter, first a discussion about the properties of equilibrium systems and the equilibrium origins of notions such as phase transitions and order parameters are provided. Then it follows with discussions about the phase transition and other important concepts in non-equilibrium systems. This chapter concludes with description of asymmetric simple exclusion process (ASEP), discussions about why it is important to the non-equilibrium community, how it is related to the other known models, and what are its exact solutions are given. Also information about its applications to



Figure 1.1: Detailed balance (a) vs steady state (b). Even though in both of the cases probability of A,B,C are all equal (when all ω 's are equal) and one third, in the steady state there is always a probability current in the clockwise direction. So steady state is a weaker condition than the detailed balance and it carries the condition of non-equilibrium systems, that is, non-vanishing currents.

the physical and other natural phenomena are shared. Chapter 3 is devoted to the discussion of shock profiles supported by Totally Asymmetric Simple Exclusion Process. Shock profiles are at the center of our findings which we present in Chapter 5. Therefore a detailed discussion about them is crucial to the completeness of this thesis. Both TASEP with single class and two-classes of particles with open boundaries are discussed. In Chapter 4, the main methodologies we used in our original work is explained in detail. These methods are master equation technique, Monte Carlo simulations and also Fokker-Planck equation. Chapter 5 consists of our original work, one of which is published in Physical Review E and the other is submitted to the same journal. Finally, Chapter 6 is the conclusion chapter. In this chapter, the summary of our findings in our original work and discussion about their impact is provided.

1.2 Equilibrium Statistical Mechanics

In statistical mechanics, equilibrium means thermodynamic equilibrium. That is, the net flux of matter or of energy inside the system or in between systems which are in contact with the system, is zero. However the required time for a system to come to equilibrium differs from system to system. Sometimes it is at the order of seconds; other times it can take so long that the distinction between equilibrium and non-equilibrium gets blurry. For instance: glass. It takes galactic years for glass to relax into the liquid state on its own.

In general, quantities such as total energy, total number of particles, or total volume, chemical potential or temperature are enough to characterize the state of the system in equilibrium. However, some states need additional variables to be completely described. Common feature of these states is broken symmetry, however other features (such as density etc) can also be used to differentiate these states. The phenomena addressed here is the **phase transition**; and the variable mentioned is the **order parameter**. This phase transition phenomena will be explained in the following section.

1.2.1 Phase Transitions

Knowledge of the equilibrium phase transition phenomena is essential for understanding the non-equilibrium phase transitions. Whereas, the former laid the foundations of the latter.

To begin with, consider a system that is composed of smaller components, such as atoms, molecules or particles. It can form stable or metastable structures as its components lose their symmetries. In other words, lost symmetries create structures. In equilibrium, one of those structures becomes thermodynamically stable (whereas other structures are metastable), *i.e.*, that particular structure corresponds to the minimum of free energy. Change in thermodynamic conditions may destabilize the equilibrium structure, and eventually another structure

becomes more stable, ergo the new equilibrium state. This change of the stability of structures is called the **phase transition** in equilibrium systems.

Phase transitions can be observed in daily life. For instance, in case of liquid-solid transition of water, by decreasing temperature one can reach from the symmetric water state to the symmetry broken ice state, or the other way around by increasing the temperature. Furthermore, ice or solid is the crystalline phase where water molecules are **ordered** in lattice structure. And water is the amorphous (structureless) liquid phase where molecules are **disordered** and symmetric. By decreasing the temperature, molecules break symmetries (lose some degrees of freedom) and become more ordered, i.e, they undergo transition from water to ice. Many phase transitions can be understood from this change of symmetry, that is to say their existence is due to **symmetry breaking**. However, not all phase transitions happen due to symmetry breaking. The liquid-gas transition of water, is an example of such transitions. Both of the states that transform during the transition, are symmetric, and they don't have a rigid structure. What differs between them is the density. Water molecules are closer to each other in liquid phase, and farther apart in gas phase.

In all of the above cases, one can define an **order parameter**, to distinguish between two different phases and observe its value through the phase transition. In the liquid-solid transition case, order parameter can be defined as the symmetry of the system. And in the liquid-gas transition case, order parameter can be defined as the density.

Likewise, toy models of equilibrium systems can demonstrate phase transitions, as well. Their demonstration capabilities of the transitions make them very convenient to understand the equilibrium phase transitions on a more controlled setting. Ising model is considered to be one of the simplest of those, it can be used to explain a significant part of the phenomena relating to phase transitions. Therefore, it is worthwhile to mention at least briefly here. For a deeper understanding, one can refer to the books [4, 5, 6, 7].

Ising is the paradigmatic model for equilibrium phase transitions. It is a 2-D

lattice model, in which each lattice point is assigned with a spin σ that can have either $+1$ or -1 values. Its Hamiltonian is of the form: $H = -J \sum_{i,j,i \neq j} \sigma_i \sigma_j$, where i, j indicates the nearest neighbors, and J is the exchange energy which has been scaled by Boltzmann constant (k_B) multiplied by temperature. (Beauty of the equilibrium statistical mechanics lies in the fact that to make predictions about system at equilibrium one does not need to take into account the dynamics of it [3]. As it is the case here, calculating its Hamiltonian gives enough information about the system.) At 0 temperature, the system is in its lowest possible (ground state) energy. This state is possible if all the spins have the same value. Though, as the temperature increases, energy also increases. And the energy increase favors changes in spin states, such that domains of spins with opposite sign appear inside the bulk. These domains disperse in the bulk as the temperature continues to rise. At the critical point, the physical picture of the bulk consists of large domains of, say for instance, plus spins enclosing smaller domains of minus spins which are enclosing domains of plus spins, and so on and so forth. This physical picture leads to important conclusions: First, the correlation length diverges at the critical point. Second, when you zoom into the picture, you always end up with the same picture with which you started with. This shows that at critical points systems become **self-similar** or in other words **scale-invariant**. Wilson discovered in 1975 (for which he was awarded with Nobel Prize in 1982) the **renormalization group theory** by employing the scale invariance. The discovery immensely availed the further understanding of criticality [8].

Along with the correlation length, closely related physical quantities, such as magnetic susceptibility and specific heat also diverge. Critically diverging physical properties of the system, exhibit a singularity $(T - T_c)^{-\alpha}$ at the critical point. Therefore when they are approaching to the critical point from below or above, they diverge. this behavior is called **power law divergence**. Usual Ising model is a static model. However, in a dynamical model with critical phase transitions, the correlation time of the system may also diverge when the system tends to the critical point. This phenomenon is called the **critical slowing down**. Moreover, together with the exponent of correlation length, all the diverging properties may have their own **critical exponents**. And they are related to each other with

scaling laws.

Another important issue about the phase transitions is the classification of them. It plays a vital role in identifying the known phenomena in completely different systems. According to Ehrenfest there are two types of phase transitions with respect to the continuity of the order parameter at the transition. If the order parameter has a jump, then the phase transition is **first order**, and if the order parameter is continuous then it is **second order phase transition**. The name first order comes from the fact that order parameter is a first order derivative of the free energy. In the case of second order phase transitions, the second derivative of the free energy is discontinuous. The aforementioned critical behaviors are characteristics of the second order phase transitions.

Fig. 1.2 displays the difference between the typical free energy diagrams for first and second order phase transitions as a function of tuning and order parameters [9]. Each well of the free energy diagram corresponds to a phase of the system. In the first order transition, system has two states one is stable (deeper well) and the other one is metastable. When phase transition occurs these phases exchanges their stability, *i.e.*, metastable one becomes stable and the stable one becomes metastable. On the other hand, in the second order phase transitions minima of the free energy corresponds to the ordered phases of the system. Upon phase transition the ordered phases merge into form a disordered phase. When approaching the phase transition, system can jump from one weakly ordered state to the other since the barrier between them is lowered, this jumping behavior is the reason behind the increased fluctuations [9] near criticality.

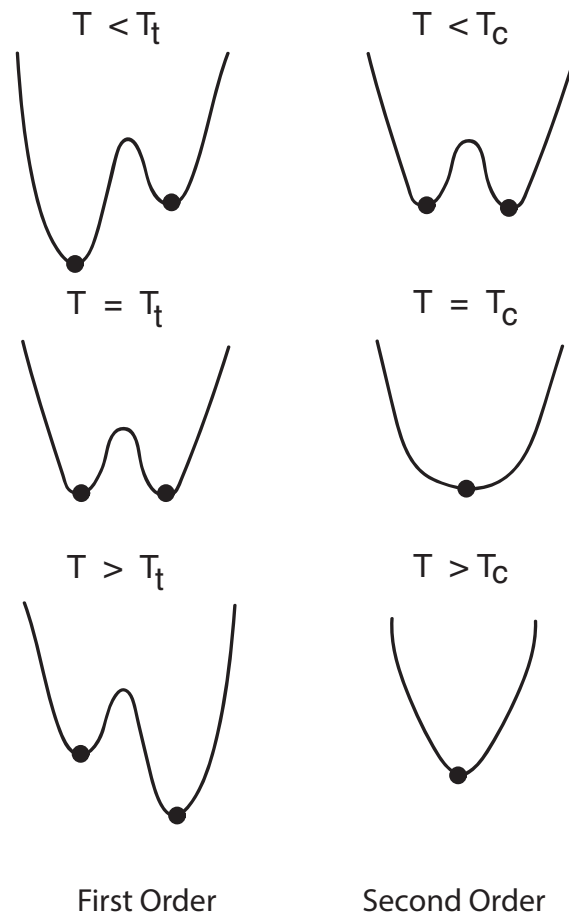


Figure 1.2: These are common schematic diagrams of free energy for first and second order phase transitions. Each well in the free energy corresponds to an ordered state. T_t corresponds to the tuning parameter of the transition, and T_c corresponds to the critical tuning parameter.

1.3 Non-equilibrium Statistical Mechanics

Despite most of our knowledge about statistical mechanics comes from studying them, equilibrium systems are more the exception than the rule. All systems exchange matter or energy with their surroundings. And the exchange is not equally reciprocated. Therefore, they yield a non-zero flux. In other words, such systems are in a non-equilibrium state. The flux can be of particle number, or of heat, or of energy etc. Nevertheless, if left alone any system should exhaust the sources of flux and come to an equilibrium with its surroundings. This process of coming to an equilibrium, **relaxation**, takes different amounts of time for different processes. Hence, non-equilibrium systems can be classified with respect to the relaxation time scales. There are different battery of methodologies of study, mostly depending on these time scales.

1.3.1 Near-Equilibrium Systems

Near-equilibrium systems, as their name gave away, are the closest to the equilibrium state. So they are the fastest to relax into it. These systems can be produced by applying small external perturbations to the equilibrium systems. Therefore, they may have the most of the characteristic properties of equilibrium state.

To study these systems, mostly linear response theory and methodologies derived from it are incorporated [10]. This is due to the fact that these systems are so close to the equilibrium state, they are considered as being in the linear regime. In this regime, all currents of the system vanish over time. Fluctuation dissipation theory (FDT) relates the system's current fluctuations with the response of the system to the perturbation [10]. The FDT can be used to predict the unperturbed system's noise or fluctuations by looking at the response to the perturbation, or by looking at the thermal fluctuations of the system it can be used to derive the response of the system [10]. These expressions can be mathematically formulated as follows: For an observable O the two-time correlation

function is

$$C(t, t') = \langle O(t)O(t') \rangle, \quad (1.2)$$

for times t and t' . Here observable average is calculated over thermal noise. And conjugated response $R(t, t')$ of the system is

$$R(t, t') = \left\langle \frac{\partial O(t)}{\partial h(t')} \right\rangle \quad (1.3)$$

where $h(t')$ is the external field applied to the system at time t' and $t > t'$. FDT relates the response and fluctuations as

$$R(t, t') = \frac{1}{T} \frac{\partial}{\partial t'} C(t - t'), \quad (1.4)$$

where T is the temperature.

1.3.2 Aging Systems

There are some frustrated phenomena in nature which relax to the equilibrium state very slowly. This process of very slow change in the system called **aging**. Aging is characterized by the breaking of time-translational invariance and the violation of FDT when relaxing. The time translational invariance implies that the functions that describe the system only depends on the time difference $t - t'$ and not the actual values of t and t' . And since in aging phenomena the time translational invariance is broken, fluctuation dissipation theory does not hold and Eqn. 1.4 depends explicitly on t and t'

$$R(t, t') = \frac{X(t, t')}{T} \frac{\partial}{\partial t'} C(t, t'). \quad (1.5)$$

These systems generally have at least two different time scales, *i.e.*, system may have fast equilibrating and very slow equilibrating properties[11].

Some of the aging phenomena happen due to **quenched**, *i.e.* frozen, disorder distributed inside the bulk of such systems. Experimentally, these disorders can be formed by super cooling the system. By cooling the system very fast, one causes the system's dynamical parameters to stick at positions where they are

not allowed to evolve themselves to the new energy of the system. The most well known example to such process is glass. It is formed by super cooling viscous liquid into the glass state, through a process called vitrification. [12, 13].

1.3.3 Far from Equilibrium Systems

Dynamics of the far-from equilibrium systems are constructed so that they do not equilibrate over finite time. These systems are the most abundant of the non-equilibrium phenomena. From turbulence to life, it is everywhere in nature.

Also there are other systems, which are designed to retain fluxes through everlasting time dependent parameters. These kind of systems are always driven to be far from equilibrium. The subject matter of this thesis is an example of such systems. We studied TASEP with time dependent boundary rates that allows to maintain non-diminishing flux in the system.

1.3.4 Steady States

Non-equilibrium steady state (NESS) is the condition where macroscopic quantities appear to be stationary, whereas a constant flux is supported throughout the system. Unlike the steady state of an equilibrium, the non-equilibrium system under steady state (SS) continues on impacting its surroundings. Mathematical expression of SS is as follows: Let C and C' be configurations of a system and $P(C)$ be the probability of configuration C then the change of probability in time is:

$$\frac{\partial}{\partial t}P(C) = \sum_{C'} P(C')w(C', C) - P(C) \sum_{C'} w(C, C'), \quad (1.6)$$

where $w(C, C')$ denotes the probability rate of transition from configuration c to configuration C' . Under steady state condition,

$$\frac{\partial}{\partial t}P(C) = 0, \quad (1.7)$$

eqn. 1.6 becomes:

$$\sum_{C'} P(C')w(C', C) = P(C) \sum_{C'} w(C, C'). \quad (1.8)$$

Equation 1.8 is the steady state condition, which is a far weaker condition than the detailed balance condition (Eqn. 1.1). However, both of these conditions give stationary probability distributions (SPD). Say here, $P^*(C)$ is the SPD of a NESS, a constant flux ($K^*(C)$) is also required to characterize the NESS. In other words, a NESS is characterized by $(P^*(C), K^*(C))$, whereas an equilibrium state is characterized by $(P^*(C), 0)$ [2].

1.3.5 Phase Transitions

As it is already mentioned, it is very hard to collect the whole non-equilibrium phenomena under the same umbrella. Since the phenomena is very vast, and so far there is no concrete, rigorous mathematical theory which unifies them. However, there are some properties that are similar to the equilibrium phenomena that we can use of to understand some of the non-equilibrium phase transitions. These are the long range order and power law scaling. Also there are phenomena that are specific to non-equilibrium systems only. These are called **emergent behavior**, such as self organized criticality or complex pattern formation.

Long range order: To follow the discussion in the equilibrium phase transitions section, I'd like to continue here with an Ising model as in the example of Racz [14]. In equilibrium, it is known that 1-D Ising model does not show any phase transitions. However, when **dynamical anisotropy** is added to the system, even the 1-D Ising displays phase transitions. This anisotropy is introduced to the system as follows [15]: two temperatures are defined so that each temperature governs the system with its own dynamics that are competing for their own equilibrium (imposed by their own temperature). These dynamics are Glauber dynamics for one of the temperatures (T_G),

$$\omega_G(\sigma' \rightarrow -\sigma) = \sum \delta_{\sigma'_1, \sigma_1} \delta_{\sigma'_2, \sigma_2} \dots \omega_i(\sigma) \delta_{\sigma'_i, -\sigma_i} \dots \delta_{\sigma'_N, -\sigma_N} \quad (1.9)$$

where ω_i is the probability of flipping the i th spin. And the Kawasaki dynamics for the other temperature (T_K):

$$\omega_G(\sigma' \rightarrow -\sigma) = \sum \delta_{\sigma'_1, \sigma_1} \delta_{\sigma'_2, \sigma_2} \dots \omega_{i,j}(\sigma) \delta_{\sigma'_i, \sigma_j} \delta_{\sigma'_j, \sigma_i} \dots \delta_{\sigma'_N, -\sigma_N} \quad (1.10)$$

where $\omega_{i,j}$ is the probability of exchanging the nearest neighbor spins (i, j). Here the energy is calculated as usual, $H = J \sum_{i,j} \sigma_i \sigma_j$. Solving the master equation for the NESS, it is shown that this system has phase transitions [15]. The results conclude, despite being constructed with short range interactions, the system displays long range ordering. In contrast to the equilibrium systems, due to complex dynamics non-equilibrium systems show long range ordering when they are away from criticality (as seen in the example even dynamical anisotropy consisting of two dynamics can create enough complexity in 1-D) [14].

Self organized criticality (SOC), is a similar phenomenon to equilibrium criticality yet there is no tuning parameter in this case. It was first introduced to model sandpiles by Bak *et al.* [16]. SOC is a property of dynamical systems that have a critical point as an attractor, *i.e.*, set of numerical values toward which a system tends to evolve. Their macroscopic behavior displays the spatial and temporal scale-invariance characteristic of the critical point of a phase transition. As it is learned from the equilibrium phase transitions, scale invariance signal long range order. The model works this way: On a two dimensional open lattice, sites are occupied by z_c number of grains. If $z_c > 4$ then the grains at that site is redistributed to the neighboring sites (**avalanche**). If the neighboring site is $z_c > 4$ then it does not get any particle from its neighbor. This redistribution of particles start from a random place in the lattice and continues until avalanche stops. Once the avalanche stops, an external source drops particles to the system until an avalanche starts again. This combination of local (redistribution) and non-local dynamics (external source adding new particles) yields a steady state. Properties such as number of active sites (s) during the avalanches, spatial size and life time of the avalanches all have power law forms $P(s) \sim s^{-\tau}$. It is suspected that, non-local dynamics is the most viable candidate for creating the long range ordering [14].

Swarming, is the collective motion of self propelled particles. In nature, flocks of birds, schools of fish, herds of land animals and swarms of insects move together in a parallel, organized way. The physical models explain these behavior is rather simple. Models assume some basic rules for individual's motion in the swarm. They assume these individuals never occupy the same place or get over-close to each other (short range repulsion), they are aligned towards the average direction and the average position of their neighbors. From these simple rules the swarming behavior of animal crowds emerge.

Pattern Formation: As previously stated, in equilibrium, systems lose symmetries and form structures, or in other words they lose degrees of freedom to form patterns. For instance, the crystalline structure of ice is a pattern. However, in non-equilibrium systems the complexity of the dynamics take part in formation of richer and much more beautiful patterns. Examples of such innumerable patterns are snowflakes, Jupiter's rings and Red spot, stripped patterns of shear flow. The most studied part of the non-equilibrium pattern formation phenomena is the deterministic systems that can be described by the nonlinear partial differential equations. Due to instabilities of these equations, patterns may form. Even for control parameters (*e.g.* boundary conditions, driving forces etc) with fixed values, nonlinear equations may have many steady solutions. Moreover, all these solutions may differ in nature. They can be isotropic, complex patterned or somewhere in between. They can exist together or individually. By tuning of the control parameter, they may emerge or disappear or lose or gain stability [17, 18].

1.4 The Model: Asymmetric Simple Exclusion Process

1.4.1 Definitions and general properties

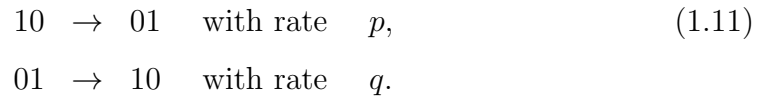
ASEP is a one dimensional driven diffusive system on which particles are allowed to hop between sites exclusively. The name ASEP carries all the critical information to determine the system's properties. It is a **process**, a stochastic one with continuous time dynamics (implying that probability of two events happening at the same time equals 0), which has no underlying energy relations. It is an **exclusion** process since only one particle can occupy a site, also known as misanthropic or hard-core repulsion relations. These relations mimic short-range interactions of real physical systems. The dynamics of the model are **simple** since when left to itself, ASEP bulk dynamics can settle down to an equilibrium state, since particles of ASEP are just random walkers. In order to drive this system out of equilibrium, one needs to create currents, therefore formation of an asymmetry is required. This could be done via coupling the bulk to particle reservoirs of different "potentials", or changing the internal dynamics. When latter is the case, random walkers become **asymmetric** random walkers [2]. In both cases one can create a current towards chosen direction.

First appearance of ASEP in the literature has occurred as a model to explain ribosomes translating along mRNA [19, 20]. Then it independently reappears again in mathematical context and named as exclusion process by Spitzer [21]. He proposed it as a Markov chain, with exclusively interacting particles. Over the course of years, it becomes the paradigmatic model for non-equilibrium phenomena and lures significant attention from scientific community.

As previously stated, ASEP is a stochastic process, that is, defining a Hamiltonian is not necessary. Kinetic approach is sufficient to explain its phenomenology [2]. It is a **Markov process**, meaning that the future evolution of the system is only defined by the configuration of the system at present time. Past has no

effect in this evolution, *i.e.*, system is **memoryless**. Moreover, it has continuous time dynamics, *i.e.* the probability distribution of the time intervals have **Poissonian** distribution. Computational equivalent of its dynamical details is **random-sequential updating** which is discussed in more detail in the Methodology chapter.

ASEP is defined on a one dimensional lattice. Particles are allowed to hop to their right if the right site is empty with probability $p dt$. And they hop to their left if that site is empty with probability $q dt$ (see Fig. 1.3 and Eqn.1.12).



The nomenclatures of different exclusion processes in this class are as follows: if $q = 0$ then bulk is called totally asymmetric simple exclusion process (TASEP). If $p > q$ it is called partially asymmetric simple exclusion process (PASEP), or if $p = q$ it is called the Symmetric Exclusion Process(SEP).

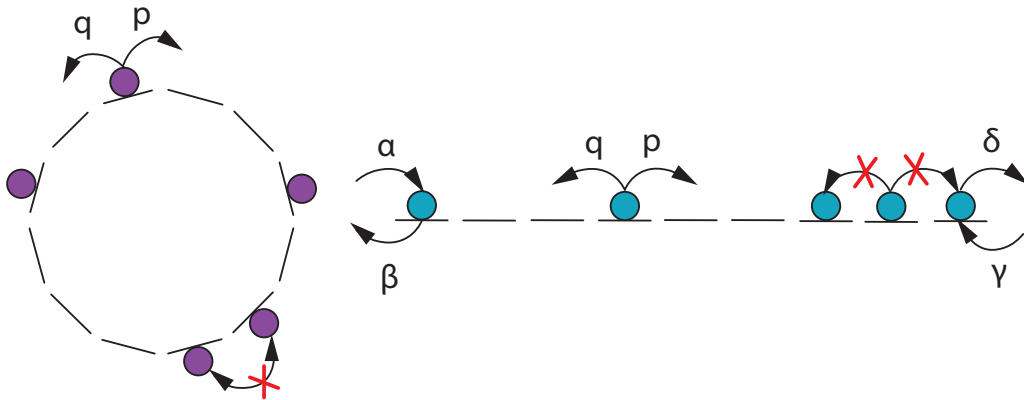


Figure 1.3: ASEP dynamics on periodic and open boundary conditions.

One can study these bulk dynamics in combination with different types of boundary conditions. The most common of those are: ring boundary conditions (simply bulk dynamics), open (finite size lattice) and infinite boundaries. In the

case of open boundary conditions particles are injected and removed from the boundaries with certain probability rates. (See Eqns. 1.13 and 1.14.)

On a lattice of size N the left-most site (site 0):

$$\begin{aligned} 0 &\rightarrow 1 && \text{with rate } \alpha, \\ 1 &\rightarrow 0 && \text{with rate } \beta, \end{aligned} \tag{1.12}$$

and at the right-most site (site N):

$$\begin{aligned} 0 &\rightarrow 1 && \text{with rate } \gamma, \\ 1 &\rightarrow 0 && \text{with rate } \delta. \end{aligned} \tag{1.13}$$

These probability rates chosen so that they match the bulk dynamics. For instance, in case of TASEP, since introducing particles from the boundary that is opposite to its hopping direction does not make sense (it cannot hop forward!), particles are injected from the boundary from where they can hop forward ($\beta = 0$) and they are extracted from the opposite boundary ($\gamma = 0$).

Moreover, there are other variations of ASEP. They may differ in construction of the dynamics as well as time update schemes (i.e, discrete time update schemes [22]). For instance, fixed hopping rates can be replaced with particle dependent [23] or site dependent rates [24]. Introducing different particle types with competing [25] (moving to the same direction) or mirror dynamics (moving to the opposite direction) [26], introducing other lanes to the system and letting particles on different lanes somewhat feel each other's presence [27] can also be done. All of those dynamics are also carefully curated to fit the relevant system they have been used to model.

ASEP is to non-equilibrium systems what the Ising model is to equilibrium systems. This is due to its non-trivial simplicity, which is albeit being exactly solvable it can still show all the crucial non-equilibrium phase transition phenomena. Additionally, ASEP has many application areas from biological to physical

transport phenomena [2], which will be discussed in the next sections.

1.4.2 Universality class, hydrodynamic limit and mappings of ASEP

Mappings can be used to identify the universal properties of models. Also, it may help building an understanding of the nature of phase transitions by examining the phenomenological differences between models as well as similarities. They may also avail the exchange of solution methods.

On the other hand, looking at the hydrodynamical limit gives an idea about coarse-grained (far less detailed) dynamics of the system over long length scales.

All the mappings that will be discussed in this section either help ASEP to be solved exactly, or help the mapped system to be understood through ASEP's known mathematical properties.

1.4.2.1 KLS Model

The Katz-Lebowitz-Spohn (KLS) model is a kinetic Ising lattice gas with attractive nearest-neighbor interactions, evolving under spin-exchange or particle-hole dynamics. It is also a paradigmatic model to the systems that are driven out-of-equilibrium. It was proposed in 1984 as a model to describe fast ionic conductors [28, 29]. The model was originally defined on a 2-D lattice where particles interact with the Hamiltonian:

$$\mathcal{H} = -4J \sum n_{x,y} n_{x',y'}, \quad (1.14)$$

where x, y labels the Cartesian coordinates of a site and $n_{x,y}$ shows the occupancy of that site and can take binary values 0 and 1, the coordinate pairs (x, y) and (x', y') denote nearest neighbors.

Stationary KLS system shows very similar phenomena to the Ising model. However it can be taken out of equilibrium by applying some drive which favors exchanges along a preferred axis. The system then begins to show curious phenomena that are vastly different from the Ising model. The only source of these

new phenomena is the breaking of the detailed balance condition [30].

In one-dimension dynamics of KLS is as follows:

$$\begin{aligned}
 0100 &\rightarrow 0010 && \text{with rate } 1 + \delta, && (1.15) \\
 1100 &\rightarrow 1010 && \text{with rate } 1 + \epsilon, \\
 0101 &\rightarrow 0011 && \text{with rate } 1 - \delta, \\
 1101 &\rightarrow 1011 && \text{with rate } 1 - \epsilon.
 \end{aligned}$$

It can be observed from these dynamics that the jump rate of the particle depends on where it hopped from and where it is hopping to. Here ϵ and δ are coefficients whose signs define whether the interaction is repulsive or attractive.

Moreover, here it can also be observed that KLS model in 1-D is a more generalized form of TASEP. In the limit of vanishing interactions, i.e, $\delta = \epsilon = 0$, these relations reduce to the bulk dynamics of TASEP.

$$10 \rightarrow 01 \quad \text{with rate } 1. \quad (1.16)$$

The KLS does not have exact solutions in any dimensions [30]. This mapping to ASEP may help to develop a method to solve it.

1.4.2.2 KPZ Universality Class

The absence of Gibbs type of distribution is the known challenge of non-equilibrium systems. Nonetheless, there are efforts to find universality classes for non-equilibrium systems. KPZ universality class is being one of them, finding its scaling distributions and limiting functions is an active research area [31].

Most of the observed stochastic phenomena obeys the Gaussian universality class. Their statistics share common properties. The fluctuations of the systems are ordered with square-root of time, at time t , as $t^{1/2}$, and their spatial distributions order with 0th order of the time, *i.e.*, they are spatially uncorrelated [31].

However, models belong to KPZ universality have different scaling exponents. Their fluctuations scale with time t as $t^{1/3}$ and their spatial correlations scale with $t^{2/3}$ [31].

In the long time and large space asymptotic limits ASEP is in the KPZ universality class. Besides, there are many other systems belong to this class [31] such as turbulent liquid crystals, fronts of burning media, facet boundaries, growth of bacteria colonies, wetting of papers.

1.4.2.3 Surface Growth Process

Surface growth process (SGP) is the simplest of the non-equilibrium systems which have both strong fluctuations and power law correlations, *i.e.*, effective criticality [14]. It is the discrete realization of KPZ equation (Eqn. 1.21) [32].

The growth of the surface, advancement perpendicular to the horizontal surface, can be simply expressed as $\partial_t h_i = v(h_i)$, where h_i is the height of the surface at site i and $v(h_i)$ is the velocity of the advancement of that surface. The model's scaling function is exactly solvable. And through its scaling functions, it belongs to the same universality class with ASEP [31].

For each configuration of the ASEP $C = (\tau_1, \tau_2, \dots, \tau_n)$, where τ_i stands for the occupation variable *i.e.* if i th site is vacant then $\tau_i = 0$, and if it is occupied $\tau_i = 1$, a unique surface profile h_j can be mapped to it such as

$$h_j = \sum_{j \leq k} (1 - 2\tau_k) \tag{1.17}$$

Schematically mapping can be done by the following procedure (See Fig.1.4): If the gradient of the height of a site i is descending then it maps to an occupied ASEP site, and if it is ascending then it maps to a vacancy in ASEP chain [32]. In the reverse mapping, hopping of a particle changes the gradient of the corresponding site, accordingly.

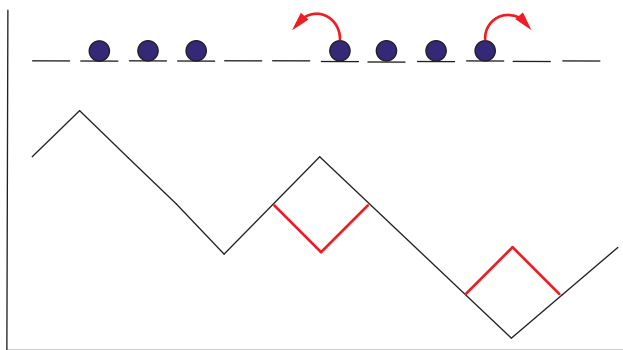


Figure 1.4: Each surface with $-\pi/4$ degree slope maps to occupied site and with $+\pi/4$ degree slope maps to a vacancy. Red lines indicates how hopping of ASEP particles will change the texture of the surface. After the hopping, slope of the occupied site becomes $-\pi/4$, and the vacant site becomes $+\pi/4$.

1.4.2.4 Zero Range Process

Zero range process (ZRP) is another driven diffusive model on a one-dimensional lattice, where particles can occupy lattice sites without any restrictions. The particles' probability of leaving their site $p_i(n)$ depend on how many particles (n) are occupying that site (i). This model is also introduced by Spitzer in his seminal paper which he introduced the ASEP as well [21]. It is widely applicable to numerous phenomena such as granular systems, interface growth, dynamics of polymers or avalanches, various transport processes, and glasses [33].

ZRP can be considered as the integrated version of ASEP. If a ZRP has N sites with M particles on it, it maps to an ASEP with $N' = N + M$ sites. Each site in ZRP mapped to a vacancy in ASEP and if a ZRP site is occupied then each particle on it maps to occupied sites that are on the left of the vacancy it mapped to. (See Fig. 1.5).

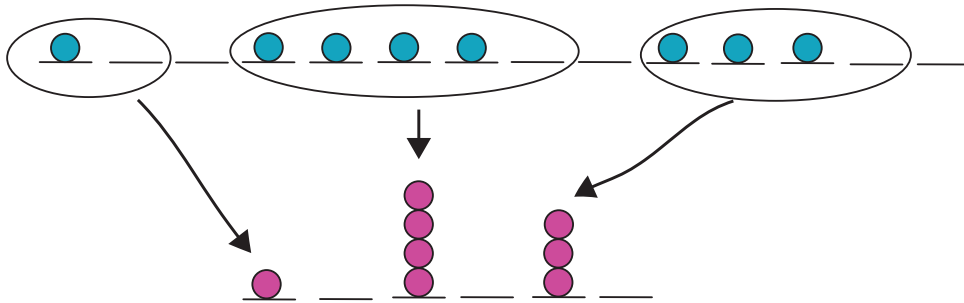


Figure 1.5: Lattice sites in ZRP mapped to vacancies in ASEP, and particles mapped to adjacent occupied sites on the left of the vacancy their site mapped.

1.4.2.5 Hydrodynamic Limit

It is known that various different one dimensional phenomena such as growth phenomena, turbulence or directed polymers in a random medium are different versions of the same problem. They can all be expressed with the KPZ or Burgers' equation. And ASEP is one of the simplest discrete realization of these equations.

Continuum equations are proposed for microscopic models in order to find the scaling limits or to observe the collective or macroscopic behaviors of such systems. Going from coarse-grained (hydrodynamic in this context) limit to microscopic scale also have advantages. For instance, the discontinuities in hydrodynamic equations signal interesting phenomena. By going to the microscopic limit, one can understand the underlying causes of it through examining the dynamics [34].

Hydrodynamic limit of ASEP was shown to be described by the inviscid Burgers' equation [35]. Starting from an ASEP model, if one rescales time and space in the same way, particle density satisfies a deterministic partial differential equation, *i.e.*, inviscid Burgers equation (IBE). One-dimensional Burgers' equation (or viscous Burgers' equation) has the following form:

$$\frac{\partial}{\partial t}\rho + \rho\frac{\partial}{\partial x}\rho = \nu\frac{\partial^2}{\partial x^2}\rho + F \quad (1.18)$$

where ρ and F are functions of x and t . And ρ is the macroscopic density, and F is an external drive. When the diffusion term is absent, $\nu = 0$, and there is no external driving, Burgers' equation becomes the inviscid Burgers' equation. ASEP is the discrete realization of the IBE, which supports shock profiles as well [36].

$$\frac{\partial}{\partial t}\rho = -\frac{\partial}{\partial x}(p - q)\rho(1 - \rho). \quad (1.19)$$

Equation 1.19 is a conservation equation, which is a paradigmatic equation for equations whose solutions can develop discontinuities, *i.e.*, shock waves. For the solution of it, initial density is defined as $\rho_o = \rho_-I_{(-\infty,0)} + \rho_+I_{(0,\infty)}$, with ρ_+ and ρ_- are being the densities right and left of the origin and are satisfying the condition $\rho_+ \neq \rho_-$. And $I_{(x,y)}$ indicates the interval between x and y . Benassi

et al showed that due to entropy condition, *i.e.*, the wave to the left should move faster than the wave to the right, there exists weak solutions to this equation [35] of the form:

$$\rho = (p - q)(1 - \rho_+ - \rho_-)t. \quad (1.20)$$

These solutions are discontinuous and has the form of a shock.

Besides there is an equation sharing the same name with KPZ universality, Kardar-Parisi-Zhang (KPZ) equation. It is a non-linear stochastic equation that describes surface growth or growing interface phenomena [37].

The KPZ equation has the following form:

$$\frac{\partial h(\vec{x}, t)}{\partial t} = \nu \nabla^2 h + \frac{\lambda}{2} (\nabla h)^2 + \eta(\vec{x}, t) \quad (1.21)$$

with noise at point x , and at time t has properties $\langle \eta(x, t) \rangle = 0$, and,

$$\langle \eta(x, t) \eta(x_0, t_0) \rangle = D \delta(x - x') \delta(t - t'). \quad (1.22)$$

Here $h(x, t)$ is the height of the surface at point x , and at time t , ν is the surface tension term, together with the $\nabla^2 h$ term it gives the relaxation or the smoothing of the surface. Second term $(\lambda/2)(\nabla h)^2$ on the RHS is the non-linear term, which accounts for the excess velocity due to local slopes.

These two equations are actually the same. Burgers' equation can be obtained from KPZ equation (eqn.1.21) by taking the gradient of the height function $\rho(x, t) = \nabla h(x, t)$, which explains why several growth processes can be mapped to ASEP.

Also note here, fluctuations of the KPZ equation, are recently proved to be in the KPZ universality class in the long time limit [31]. However, scaling of its spatial correlations are still unknown.

1.4.2.6 Quantum Mappings

ASEP on a ring (that is to say, ASEP's bulk dynamics) can be mapped to spin $1/2$, anti-ferromagnetic XXX($J = J_x = J_y = J_z$) Heisenberg chain with non-Hermitian matrices (due to the asymmetry of the motion)[38]. Equivalently, it can be mapped to the 1-D Ising model, where spins are interacting only in the z-direction and with a transverse magnetic field is in the x-direction. Realization of the quantum mappings lead to the employment of Bethe ansatz on the ASEP problem on a ring [2]. It enables exact calculations for problems related to the spectrum of Markov matrix of ASEP [38].

1.4.3 Exact Solutions

ASEP is an exactly solvable model. The most significant of the solution methods are the matrix product ansatz (MPA) and Bethe ansatz [38].

MPA was introduced by Derrida *et al* for TASEP with open boundaries [39]. It is based on the quantum inverse scattering technique [2, 40]. It has non-commuting operators, each assigned to different sites of the lattice. These operators can be of two types, one type is for the occupied sites, and the other one is for the vacancies. Provided that the quadratic algebra relations are satisfied, these matrices give the exact steady state distribution of TASEP [39]. The technique further enabled the calculation of current fluctuations [34], equal time correlations and large deviation functionals [41]. Also by utilizing this technique Speer proved that the steady state distribution of ASEP with two species of particles is not a Gibbs measure [42].

Second technique is the Bethe ansatz which is traditionally employed in finding exact solutions for one-dimensional quantum many-body systems. Application of the ansatz to 1-D stochastic processes was first done by Dhar [43]. As discussed in the previous section ASEP can be mapped to several 1-D quantum systems. These mappings hint the application of Bethe ansatz to these systems is possible.

It availed the extraction of information about the spectrum of the Markov matrix [2] and the related information such as its spectral gap [44, 45, 46, 47] and large deviation functions [48, 49, 50]. From the spectral information, it is also found that the relaxation time scales as $T \sim L^z$ with the dynamical exponent $z = 3/2$, where L is the system size. This exponent is the same with the KPZ equation's relaxation exponent [2].

There are also other mathematical methods applied to ASEP. Some of these are: [2]: quadratic algebra [51], Young tableaux [52], combinatorics [53], orthogonal polynomials [54], random matrices [55], determinantal representation [56].

1.4.4 Applications

From the first time it was introduced in 1968 as a model for RNA translation by ribosomes [57], ASEP is used as a model for various biological transport phenomena, as well as vehicular transport and some of chemical diffusion problems. Modeling of those systems with the mathematically very well established ASEP provides an opportunity to understand the dynamics of those systems.

1.4.4.1 Biology

For models in biophysical systems, often the usual ASEP combined with necessary dynamics is used for better explaining the system. For instance, modeling ribosomes on mRNA or molecular motors (protein structures which carry cargo on a microtubule (filament-like protein structure that forms cytoskeleton), one needs an adjustment to the dynamics such that several lattice sites occupied at once. Moreover, in both of the aforementioned systems particles tend to detach from the system even before they reach the end. So introducing detachment (or also may be the attachment) type of dynamics to the model (Langmuir kinetics) becomes necessary [2].

On the other hand, in case of co-transportation of molecules, new species of

particles can be introduced to the system. And these new species may compete or work cooperatively with each other, that defines conditional transition rates for ASEP particles [2]. If the particles, *e.g.* molecular motors, can pass along each other, then partial exclusion dynamics may be introduced to the system. Or if the particles are able to interact among different lanes then other lanes can be introduced to the system with certain interaction rates. These properties are again crucial in modeling the molecular motor behavior in cellular transport [2].

ASEP with free or dynamical boundary conditions can also be constructed. Such a system can be used to model the growth model of filaments of fungi [58, 59]. When growing, filaments of the fungi elongate, and their cytoplasm moves to the direction of advancement which is made possible by the elongation of the cyto-skeleton to the same direction. This motion is modeled by the carriage of building blocks of micro-tubule to the tip of the existing cyto-skeleton [58].

1.4.4.2 Physics and Chemistry

In physics and chemistry the single-file diffusion or any other diffusion structure that can be reduced to single-file diffusion can also be modeled by ASEP.

Diffusion in zeolites can be a good example of chemical transport through porous networks. In general, light hydrocarbons diffuse inside zeolites. However, upon diffusing particles may chemically interact with the atoms of zeolites interacting among themselves. If the interaction among the particles is attractive and it is larger than the interaction between particles and zeolite atoms, then the particles diffuse inside the zeolite. Also the ease of diffusion when another particle is adjacent can be incorporated into ASEP as the increasing jump probability rate when another particle is present [60].

Likewise, there are many other phenomena, mostly on different narrow channel transport systems, that ASEP is utilized to model. Some of them are conductivity of solid electrolytes [61], thin vessel transport of macromolecules [62], repton

model of polymers in a gel [63], traffic and granular flow [64], stochastic surface growth [65, 66], sequence alignment of genes in computational biology [67], pedestrian queuing [68], and also some problems in large networks [69].

Chapter 2

First order phase transitions: Shock profiles

TASEP is one of the simplest of non-equilibrium systems. It is composed of asymmetric random walkers on a one dimensional lattice that interact exclusively. In equilibrium systems, boundaries does not play significant role in any phase transitions [70]. However, Krug showed that if particle flux is present even in one-dimensional lattice systems phase transitions that are induced by boundaries can occur [71].

Although a thermodynamic free energy function cannot be defined for non-equilibrium systems, (which is needed to characterize the order parameter in equilibrium systems: the first order derivative of the free energy is the order parameter), an order parameter can still be defined. In non-equilibrium systems, the parameter is chosen so that it can define the observed differences between states. For instance in TASEP, density parameter describes the difference between the low density and high density states. It jumps (as in the form of a shock) upon the boundary between the states which indicates a first order phase transition.

The shock in TASEP, also known as **domain wall** or **interface**, implies an average density profile that has the shape of a hyperbolic tangent or of an error

function [70]. The width of the domain wall (the transition region between high and low density, it i.e., upper and lower branches of the hyperbolic tangent) is small-scaled compared to the lattice size [70].

2.1 Single Class of Particles

One species TASEP with open boundaries is a one dimensional lattice which is attached to two particle baths from its ends. One of the baths supplies particles (here the left bath) to the system and the other one acts as a particle sink (right bath). From the left bath, particles are allowed to enter the system with probability rate α if the left most site is empty. They hop forward with probability rate γ , provided that the next site is empty. And when they reach the right most end, they exit the system with probability rate β . (See Fig.2.1.) In order to fix the time scale of the system, every probability rate is scaled with (divided by) γ , and γ is set to 1. Final dynamics are:

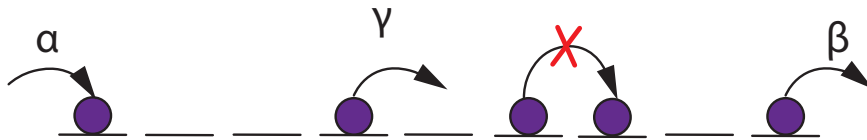
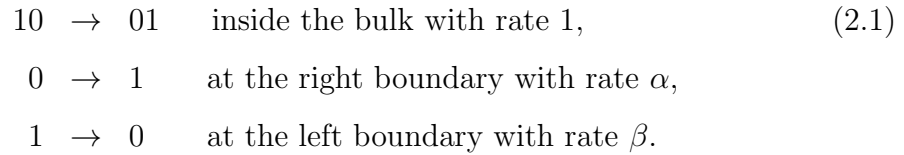


Figure 2.1: One species, open boundary TASEP model.

2.1.1 Phase Diagram

TASEP is an integrable model (*i.e.*, it is exactly solvable). In their seminal paper, Derrida *et al* exactly solved it by implementing a matrix product ansatz [39]. Its steady state probabilities are found with respect to the boundary rates [39]. Hence, its phase diagram is also known. Three different phases of the system are identified with respect to the particle entry (α) and exit (β) rates: These are low density (LD), high density (HD) and maximal current (MC) phases.

In this system, order parameter is the density (d). The LD phase has density $d < 0.5$ and the HD phase has density $d > 0.5$. The phase transition from LD to HD phase is first order. Moreover, in the MC phase density is $d = 0.5$, and the current reaches its maximum value $j = 0.25$. Phase transitions among HD-MC and LD-MC are second order. In the phase space these phases are located: LD at $\beta > \alpha$ and $\alpha < 1/2$, HD at $\alpha > \beta$ and $\beta < 1/2$ and MC is at $\alpha > 1/2$ and $\beta > 1/2$ (See Fig. 2.2).

In the HD phase low exit rate controls the bulk density. Since particles enter faster than they exit the system, they start to accumulate. Therefore, density of the system is controlled by the exit rate and it is $1 - \beta$. Similarly, in the LD phase low entry rate limits the bulk density and it is equal to α . Particles exit the lattice faster than they enter. Bulk density stays low. On the other hand, in the maximal current phase particles enter and exit in fast rates. Density of the bulk remains 0.5, and the current is at its highest 0.25 all the time. Table 2.1.1 shows the density and current values of these phases as functions of boundary parameters.

phase	density	current
MC	$\frac{1}{2}$	$\frac{1}{4}$
HD	$1 - \beta$	$\beta(1 - \beta)$
LD	α	$\alpha(1 - \alpha)$

Table 2.1: Density and current values that correspond to the phases of TASEP.

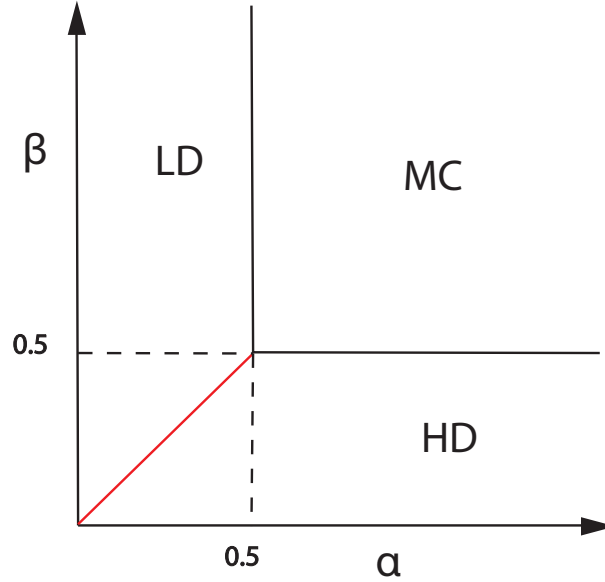


Figure 2.2: Phase diagram of TASEP with single species, with open boundary conditions.

2.1.2 Shock Profile

On the coexistence line between the HD and LD phases ($\alpha = \beta < 1/2$), density profile of the system has the form of the shock. In order to visualize a single realization of the domain wall, think of the situation where boundary rates are very small, *i.e.*, $\alpha \ll 1$ and $\beta \ll 1$. Under such conditions after a while, all the particles pass the vacancies and accumulate to the exit boundary. The configuration of the system eventually will consist of a domain of vacancies and a domain of particles : (...0000011111...). If a particle can jump out of the system, then the rest of the particles arrange themselves so that the domain wall move to the right by one site. Or if a new particle enters the system, then again the domain rearranges itself and the domain wall move one site to the left. The shock profile is time average of these single realizations of the domain wall (See Fig. 2.3)

As discussed in the introduction, hydrodynamic (continuum) limit of the TASEP is inviscid-Burgers equation, which has the form:

$$\frac{\partial}{\partial t} \rho = -\frac{\partial}{\partial x} \rho(1 - \rho). \quad (2.2)$$

Given asymmetric initial densities, left ρ_L and right ρ_R , obeying the condition $\rho_R > \rho_L$, there exists traveling wave solutions of this equation $\rho(r - vt)$ [72, 73], with velocity v , and v is

$$v = (1 - \rho_L - \rho_R). \quad (2.3)$$

Similarly, if asymmetric initial conditions are given to TASEP satisfying the same condition as IBE (...000011111...), the structure persists. However, if one gives the opposite initial configuration (...1111100000...), the structure quickly diffuses[36], even though in both cases currents are 0 inside the domains. However, in the second configuration it can be seen that the system's dynamics enable hopping at the interface. Therefore, in the course of time it diffuses. These results shows that shocks are stable structures of the dynamics.

Ferrari showed that position of the domain wall can be tagged by introducing a novel type of particle into the system [74]. He defined the dynamics of this novel class (2) of particle as

$$\begin{aligned} 10 &\rightarrow 01 \\ 20 &\rightarrow 02 \\ 12 &\rightarrow 21. \end{aligned} \quad (2.4)$$

Observe here that, due to its dynamics after sufficient time has elapsed before measuring, this particle will be found at the domain wall (...00000211111...). Therefore, it will tag the position of the shock. He showed that the velocity $r(t)/t$ of the tag particle converges to Eqn.2.3 [74] where $r(t)$ is the position of this particle at time t .

Moreover, the particle number can take a wide range of values on the co-existence line. Therefore, the shock profile is doing a biased random walk on the lattice. From the perspective of the second class of particle, Schutz showed that [36] velocity of the shock profile is

$$v = \frac{J_R - J_L}{\rho_R - \rho_L}, \quad (2.5)$$

and the diffusion constant is

$$D = \frac{1}{2} \frac{J_R + J_L}{\rho_R - \rho_L}, \quad (2.6)$$

where J_R and J_L are currents and ρ_R and ρ_L are densities for left side and right side of the shock.

As a side note, on the coexistence line taking ensemble averages of the occupation numbers of the sites does not yield any physically realizable observable [75]. By averaging out the densities that corresponding to all particle numbers, the measurements flatten out the shock profiles and results with a linear density profile.

Interestingly, Schutz [76] suggested a much more simplistic model of ASEP which also displays shock behavior. He suggested a model in which particle dynamics are stochastic at the boundaries, but it is deterministic inside the bulk. In other words, the system he suggests has parallel lattice dynamics. The phase diagram has only two phases of low and high densities. They are located at the first-quadrant of α vs β graph. The transition is on the $\alpha = \beta$ line. Again, as in the TASEP, along the phase transition line one can observe the HD-LD shock structure.

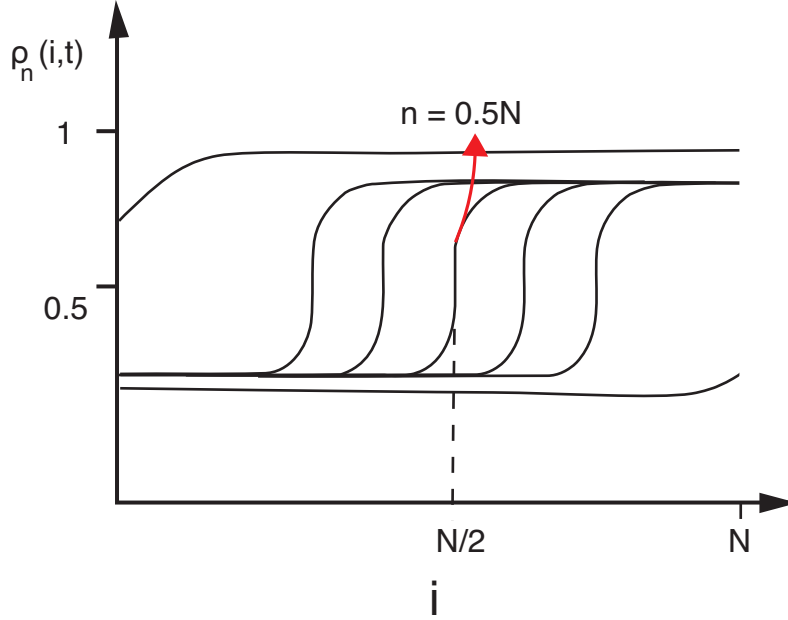
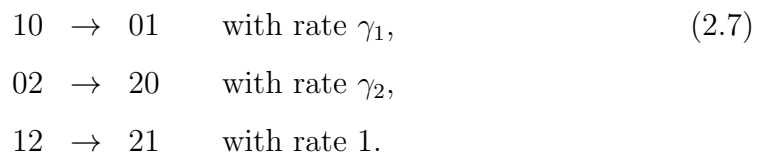


Figure 2.3: Shock profile for different numbers of particles in a lattice of 50 sites. i indicates the site, $\rho_n(i)$ indicates the density profile that corresponds to the n number of particles.

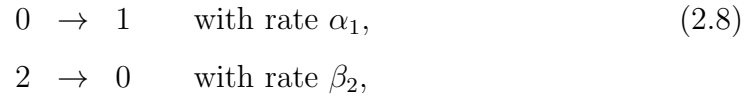
2.2 Two Classes of Particles

In the case of TASEP with two classes of particles, second class of particles are introduced to the system with same dynamics but they are only allowed to move in the opposite direction. Second-class of particles enter the system from the right most end, if that site is empty with rate α_2 . They can hop forward (to the left), if the next site is empty, with probability rate γ_2 . And when they reach to the left most site, they can exit the system with rate β_2 . If these two classes of particles come face to face, they exchange their sites with probability rate δ . Here for the time scaling every probability rate is divided by δ and δ is set to 1. Figure 2.4 shows the schematic description of the model.

Inside the bulk,



At the right boundary,



and finally at the left boundary,

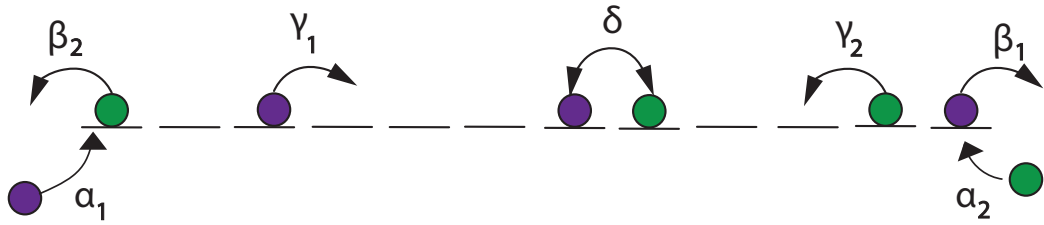
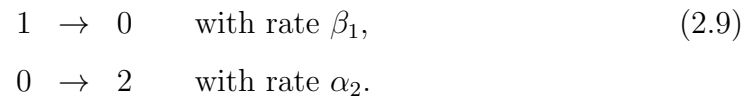


Figure 2.4: Schematic description of TASEP with two species of particles under open boundary conditions.

2.2.1 Phase Diagram

The phase diagram of this model is not exact since there is not any exact solution to this model so far. Evans *et al.* calculated the phase diagram (see Fig. 2.5) through mean field (MF) analysis and supported their findings with Monte Carlo analysis [77].

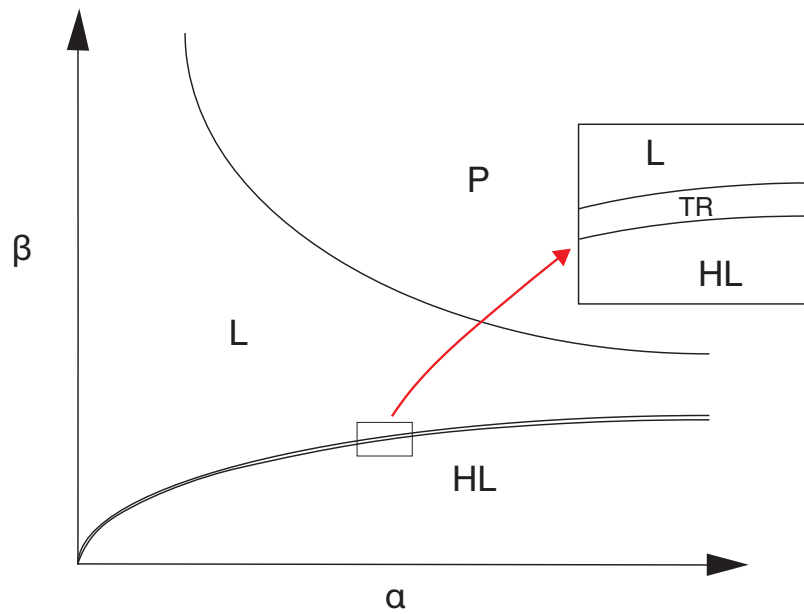


Figure 2.5: Mean field phase diagram of TASEP with two types of particles. Here $\alpha_1 = \alpha_2 = \alpha$, $\beta_1 = \beta_2 = \beta$ and $\gamma_1 = \gamma_2 = \delta = 1$.

The MF analysis indicates that there are four phases in the phase diagram with respect to the density. In their case, all parameters are chosen to be symmetric, such that $\alpha_1 = \alpha_2 = \alpha$, $\beta_1 = \beta_2 = \beta$. Other parameters are set to 1, $\gamma_1 = \gamma_2 = \delta = 1$. Starting from the lower values to the higher values of β , these phases are (see Fig. 2.5): symmetry broken HL (high density (HD)- low density (LD) phase, “tiny regime” (TR), the L (LD-LD) phase and the power law (P) phase. In the HL phase even though all the parameters are symmetric for both of the particles, system displays spontaneous symmetry breaking. This is the first one-dimensional non-equilibrium model, which is reported to display spontaneous symmetry breaking [78].

To be able to understand the nature of the phases it is better to look at the Evans *et al*'s MF solution first [77]. Here $\tau_j = i$ is the occupation variable at site j where $i = 0, 1, 2$ and these values correspond to vacancies, first or second class of particles in the respective order. In the MF approximation, $P(\tau_1, \tau_2, \dots, \tau_N) = P(\tau_1)P(\tau_2) \dots P(\tau_N)$. Note also that if all bulk rates are equal $\delta = \gamma_1 = \gamma_2$, then particles cannot distinguish between the other class of particles and vacancies. Therefore, particles' motion decouples inside the bulk. On the other hand, they are still coupled at the boundaries. Here, $p_{1,j}$ is the probability of first-class particle occupying site j , and similarly $p_{2,j}$ is the second-class particle occupying the same site. Evans *et al* ended-up with the simplified MF equations of the system. In the bulk, result of the exact solution to the decoupled TASEP (with one class of particles) is used. These solutions are then coupled to one another using MF approximation. And coupling of the two TASEP at the boundaries yields the effective boundary rates:

$$\begin{aligned}\alpha_1^{eff} &= \alpha(1 - p_{1,1} - p_{2,1})/(1 - p_1) = J_1/(J_1/\alpha + J_2/\beta), \\ \alpha_2^{eff} &= \alpha(1 - p_{1,N} - p_{2,N})/(1 - p_2) = J_2/(J_2/\alpha + J_1/\beta).\end{aligned}\tag{2.10}$$

In the end, first class of particles act as an individual TASEP with boundary rates (α_1^{eff}, β) and the second class of particles act as another individual TASEP with boundary rates (α_2^{eff}, β) . I would like to note here that we carried out a more conventional MF analysis and its solutions also confirmed their results.

Now, the phase diagram can be understood from this perspective. Phases are

superposition of the phases of individual ASEPs. For instance, in the power-law phase both systems are symmetric and they are in MC phase. In the L phase, both systems are symmetric and they are in LD phase. However, in the first (it is the first one since we are counting the phases starting from the high values of β to lower values) symmetry broken phase TR, even though both systems are subject to the same boundary conditions they are in different LD phases. Both of their densities are below 0.5 but they are not equal to each other. Finally, the symmetry broken phase, even though all parameters are equal one class of the particles dominate the system. This happens due to the accumulation of those particles to the exit, and not letting the other class of particles to enter the system. Eventually, accumulating particles dominate the system (HD phase), and the other particles get to be in LD phase.

Phase transition between the symmetric L and P phase is second order. Whereas, there are various claims about the order of the transition from the symmetry broken phases to the symmetric L phase. Some even claim that the TR phase is not a real phase but a finite size effect [79]. Arndt *et al* further claimed that TR phase does not exist, and there is a first-order phase transition from HL to L. Both of their argument rely on MC simulations [80]. Finally there is the third view, that we also came to agree during our studies, which claims that the TR phase exists and there are two first order transitions, one is from HL to TR and the other is from TR to L. However, these transitions have different natures [81]. The two symmetry broken phases HL and TR can exist at the same time, since they both have the same current. However, TR and L phases never coexists due to the fact that their currents are not equal [81].

2.2.2 Shock Profile

Shock profiles can also be observed when second class of particles are present in the system. As previously stated, under the condition of equal bulk rates, the system can be thought of as two different TASEPs which are coupled at their boundaries.

At the TR, the two phases HL and TR can coexist together. One can see this in Fig. 2.7. Here, the first-class particles display the shock profile, *i.e.*, they have high density in some parts of the lattice, and at the other parts they have low density. Whereas, second class of particles always have lower density than of the first class of particles. In the left part of the lattice, the lower part of the shock of first-class of particles and the low density second-class particles exist together, *i.e.*, the system is in TR phase for this part of the lattice. However, in the left part of the lattice, first-class of particles are in higher density and second-class of particles remain in their low density state. Then, this part of the lattice is in HL phase (See Fig. 2.6).

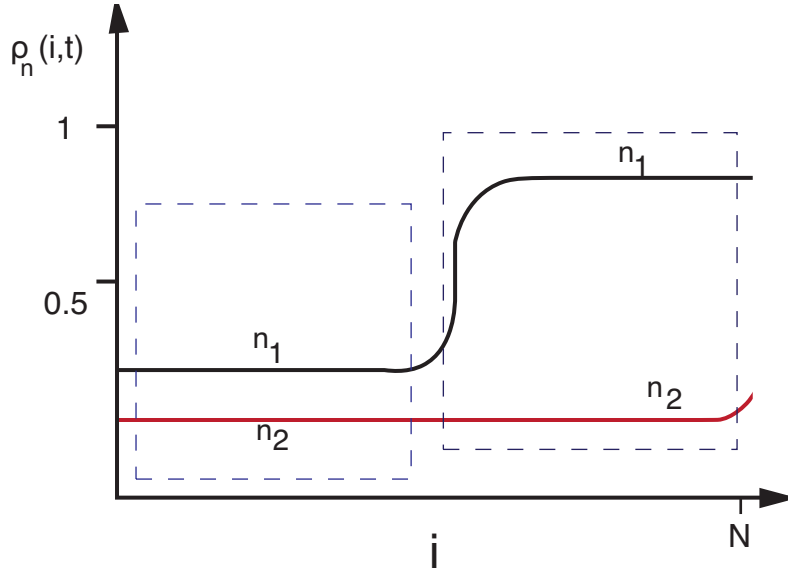


Figure 2.6: Schematic density vs lattice plot for TASEP with two classes of particles. In the left box the lattice is in TR phase. However on the right box it is in HL phase. It displays that these two phases can coexist.

The whole phase structure for lower values of β can be understood as the clogging of the first-class particles to the right end. Suppose entrance rate is fixed and it is bigger than β . For increasing values of β , the shock profile moves to the right and the domain in the lattice, where HL and TR phases coexist, increase. At some point, β becomes sufficiently large enough that there will be no clogging in the system. After that point, eventually the system reclaims its symmetry (L phase), since every rate is symmetric for the two classes of particles.

Note here, before reaching the L phase β is significantly smaller than the bulk rate 1, so first-class particles have time to rearrange themselves as a domain when particle number changes. Moreover, the shock-profile moves to the right or to the left depending on the entry or exit of a particle.

This discussion about the phase transitions for low-values of β may also indicate that the TR phase always exists, but it may exist for narrower values of β . This conclusion can further be backed-up by the work of Erickson *et al* [79] as a residual point-like interval of β vs density difference as an indicator of the TR phase.

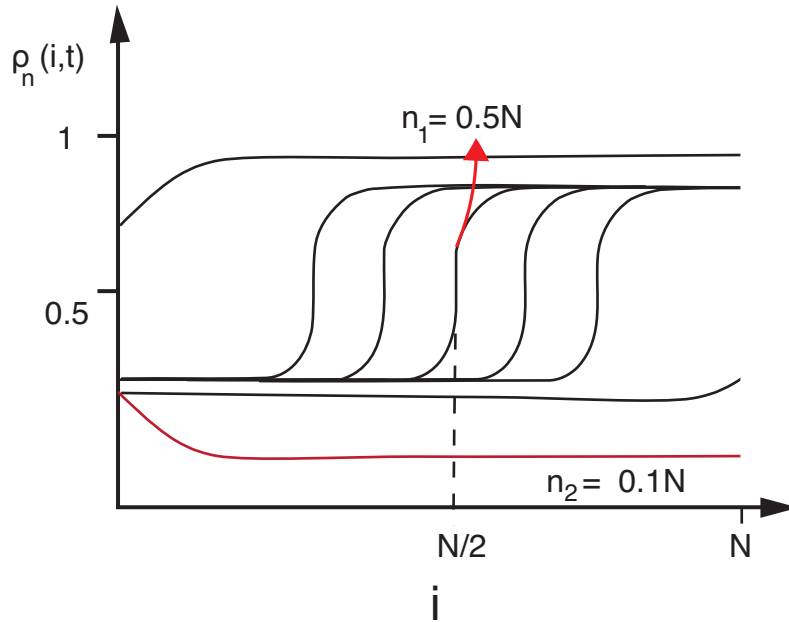


Figure 2.7: Schematic density vs lattice plot for TASEP with two classes of particles. First-class particles display the shock profile, for various numbers of particles in the lattice. Whereas, the second-class particles remains in low density state (LD).

Chapter 3

Methodology

The methodologies that were used throughout this thesis are the numerical solutions of the master equation and the Fokker-Planck equation as well as the kinetic Monte Carlo technique. Relevant details about each of these methods will be supplied in this chapter.

3.1 Master Equation

Master equation is the fundamental equation that carries the complete information about the time evolution of a Markov process. A Markov process has no-memory of its history. The future of the system only depends on the current state of it. A master equation can describe the evolution of the system in time and how the transitions occur between its states until the system reaches a steady state. In this state, probability of the system does not change. However, not all systems can reach a steady state.

ASEP is a Markov process. Its realizations are connected to one another through probability rates. A single realization can be the future of a certain realization and also it can be the past of another realization. This connectedness manifests itself through probability rates of transitioning from one to the other.

Master equation carries all these rate information.

In mathematical terms, say a single realization of ASEP is c , and the probability rate of transition from c to another realization c' is $\omega(c \rightarrow c')$. A transition means hopping of a particle in the system. At a time interval dt , the probability of the hopping is $\omega(c \rightarrow c')dt$. Then the master equation which defines the rate of change of the probability of the configuration c can be written as follows:

$$\frac{\partial}{\partial t}P(c, t) = \sum_{c \neq c'} P(c', t)\omega(c' \rightarrow c) - \sum_{c \neq c'} P(c, t)\omega(c \rightarrow c'), \quad (3.1)$$

provided that $\sum_c P(c, t) = 1$. This equation can also be expressed by a matrix representation. The transition rates of the matrix is called Liouville operator (\mathcal{L}). And the probability \mathcal{P} is the vector that carries the information about the probabilities of all possible configurations :

$$\frac{\partial}{\partial t}\mathcal{P} = \mathcal{L}\mathcal{P}. \quad (3.2)$$

This Liouville operator carries all the information about the time evolution of the system.

The condition that the probability is not changing with time ($\partial\mathcal{P}/\partial t = 0$) is the steady state condition. It corresponds to the zeroth eigenvalue of Liouville operator:

$$\mathcal{L}\mathcal{P} = 0. \quad (3.3)$$

For a sufficiently small system size Eqn. 3.3 can be solved analytically by techniques such as generating function method or by directly solving the matrix equation. However, latter is not possible for majority of the cases, since the size of the matrix get enormous very quickly. For instance, for an ASEP with lattice of size N , its Liouville operator will be of size $2^N \times 2^N$. Even on the order of 10, this matrix becomes too big to directly solve with computers.

Some other relevant properties of the Liouville operator of ASEP are as follows [2]:

- Values of rows of each column of \mathcal{L} add up to 0, due to the conservation of probability.

- \mathcal{L} is not Hermitian therefore its right and left eigenvectors are not conjugate pairs.
- For finite ASEP, \mathcal{L} is ergodic, so that its biggest eigenvalue is 0 and other eigenvalues are negative.
- Right eigenvector corresponding to the 0 eigenvalue, consists of steady state probability values of each micro-state. Namely steady state is a dynamical state, *i.e.*, system is visiting all micro-states with the frequencies (probabilities) registered on steady state vector.
- Perron-Frobenius theorem guarantees that the biggest eigenvalue is non-degenerate. Therefore, steady state is unique.
- Steady state is dynamic. Thus, microscopic fluctuations can be observed as well.
- Steady state carries a fixed current along the lattice, whose value depends on the boundary rates. This implies boundary induced phase transitions [71].

3.2 Monte Carlo Analysis

A Monte Carlo (MC) simulation is a probabilistic experiment that can be used to achieve results about a systems properties. Those systems are often too complicated to solve with other methods. MC has a very wide-range of applicability in physics from modeling many body stochastic [82] or quantum systems [83] to otherwise non-soluble integrals [84]. The method was invented by Stanislaw Ulam and Nicholas Metropolis in 1940s, when they are working on the nuclear weapon project. The method is named after the famous casinos of a small town named Monte Carlo, France [85].

Master equation (Eqn.3.1) can be directly simulated by **random-sequential update** MC analysis, that is to say particle positions are updated randomly

at each (continuous) time step. Probability of a configuration can be reached through the frequency of appearance of that configuration during the course of the simulation. The transition rates between the configurations (hopping rates in case of ASEP) are taken as input to the algorithm which are simulated by using random numbers. If it is guaranteed by the master equation itself, the simulated average probability of the configuration reaches a steady state (probability does not change). Macroscopic steady state properties of the system can be calculated from this probability.

Moreover, there may be other computational update schemes of the same system that correspond to different steady states. (Here I say the same system in a sense that some of the basic dynamics of the systems are equivalent such as particle exclusion, or boundary injection or extraction rules etc.) For instance ASEP has other computational update schemes which correspond to discrete time dynamics. These are ordered sequential, sub-lattice-parallel and parallel update schemes[86, 32].

Say (i, j) are the lattice site indexes of update pairs, in ordered sequential update scheme starting from left (or right end) of the lattice, $(i = 1, j = 2), (i = 2, j = 3), (i = 3, j = 4), \dots$, are updated in that (or reverse) order. If it is an open boundary ASEP, a particle may enter (or leave) the system after all the updates are finished [86]. On the other hand, in the sub-lattice-parallel update the lattice size must be an even number. First boundary hoppings are carried out. Then even pairs are updated, such that $(i = 2, j = 3), (i = 4, j = 5), (i = 6, j = 7), \dots$, until it reached the opposite end. After that odd pairs are updated $(i = 1, j = 2), (i = 3, j = 4), (i = 5, j = 6) \dots$. This is a computationally efficient scheme and theoretically it corresponds to a transfer matrix representation with local products [86]. Finally, in the case of parallel-update scheme, all the system is updated at the same time (bulk hopping, particle entrance and exit). This scheme leads to the strongest of correlations, therefore it is most commonly used to simulate traffic systems [86].

Note here that for analytic purposes random-sequential update should be chosen. However, computationally discrete time update schemes are more effective

[86]. Hence, examining the advantages and disadvantages before proceeding to carry out a simulation has critical importance.

3.3 Kinetic Monte Carlo

Kinetic Monte Carlo (KMC) algorithm is typically used to simulate time evolution of systems which have transition rates defined among configurations. The method is also known as dynamical Monte Carlo method.

In this algorithm transition rates are predetermined. They are not reached through the simulations. In case of ASEP, transition rates are particle entry (α), exit (β) and bulk hopping rates ($\gamma = 1$). In the course of simulation which particle will hop next is chosen randomly (random sequential update). This random update process is carried out as follows: At a given instant, all allowed hopping (exit and entry included) rates (ω_i) are summed, such that $\Omega = \sum_i \omega_i$. Then a random number r (uniformly distributed between 0 and 1) is drawn and the incremental time Δt is calculated as $\Delta t = -\log(r_1)/\Omega$. This incremental time corresponds to the necessary time to be elapsed before system to lose its current configuration. Note here that, continuous time dynamics in this setting correspond to a Poissonian process. That implies events happen instantaneously that no two transitions can happen at the same time. Therefore incremental time (the waiting time of the configuration (Δt)) has an exponential distribution. After the waiting time has elapsed, a particle i is chosen randomly if $\Omega_{i-1} < r\Omega < \Omega_i$. Here r is another random number which is uniformly distributed between 0 and 1. Algorithm 1 displays the pseudo-algorithm for this process.

Algorithm 1: Kinetic Monte Carlo pseudo-algorithm for ASEP with oscillating boundary rates

Initialize time
 Start a MC Step
 Start a full lattice swipe
 Calculate Ω at curret time
 Draw a random number r_1
 Calculate incremental time as:
 $\Delta t = -\log(r_1)/\Omega$
 Draw another random number r_2
 Choose a particle to hop as:
 $\Omega_{i-1} < r_2\Omega < \Omega_i$
 Measure the current and density averages.
 Repeat until all MC steps are exhausted.

3.4 Fokker-Planck Equation

The Fokker-Planck (FP) equation [87, 88, 89, 90, 91] describes the time dependence of the probability distribution $P = P(x, v, t)$ of the position and velocity of a Brownian particle inside a potential well $V(x)$. The FP equation has the general form

$$\frac{\partial P}{\partial t} = -v \frac{\partial P}{\partial x} + \frac{\partial}{\partial v} \left[\left(\frac{\gamma}{m} v - \frac{1}{m} \frac{dV}{dx} \right) P \right] + \frac{D}{2m^2} \frac{\partial^2 P}{\partial v^2}, \quad (3.4)$$

where D is diffusion and γ is drift constant.

Furthermore the FP equation for over-damped systems can be derived from the **Langevin equation** (LE) [5]. LE is the equation that describes the motion of a Brownian particle inside a potential well $V(x)$,

$$m\ddot{x} = -\gamma\dot{x} + F(x) + \eta(t), \quad (3.5)$$

where force is $F(x) = -dV(x)/dx$. In the limit of strong friction, velocity of the Brownian particles relax to the stationary state very quickly and variations of their velocities are negligible $\ddot{x} \sim 0$. Then the Eqn. 3.5 reduces to

$$\dot{x} = \frac{1}{\gamma} F(x) + \frac{1}{\gamma} \eta(t). \quad (3.6)$$

where $\eta(t)$ is chosen to be a Gaussian white noise with properties $\langle \eta(t) \rangle = 0$ and $\langle \eta(t_1)\eta(t_2) \rangle = D\delta(t_1 - t_2)$.

Moreover, probability of finding Brownian particle in the interval $x \rightarrow x + dx$ at time t is $P(x, t)$. And we know that the continuity equation of probability density $\rho = \rho(x, t)$ of the particle is

$$\frac{d}{dt}\rho + \nabla \cdot j = 0, \quad (3.7)$$

where j is the probability current $j(x, t)$, which is $j = \rho\dot{x}$. By substituting the LE (Eqn. 3.6) into the continuity equation (Eqn. 3.7), one gets

$$\frac{\partial}{\partial t}\rho = -\frac{\partial}{\partial x}(\dot{x}\rho) = -\frac{1}{\gamma}\frac{\partial(F(x)\rho)}{\partial x} - \frac{1}{\gamma}\eta(t)\frac{\partial\rho}{\partial x}. \quad (3.8)$$

Note here that $\rho(x, t)$ changes with respect to the stochastic variable $\eta(t)$. Hence a macroscopic probability density $P(x, t)$ can be defined as $P(x, t) = \langle \rho(x, t) \rangle_\eta$, which is the average probability density over all values of noise η . Let's define, time-independent deterministic operator \widehat{D} and time-dependent stochastic operator $\widehat{S}(t)$ such that

$$\widehat{D} = \frac{1}{\gamma}\frac{\partial F(x)}{\partial x} + \frac{1}{\gamma}F(x)\frac{\partial}{\partial x}, \quad (3.9)$$

and

$$\widehat{S}(t) = \frac{1}{\gamma}\eta(t)\frac{\partial}{\partial x}. \quad (3.10)$$

Then Eqn.3.8 can be written as

$$\frac{\partial}{\partial t}\rho = -\widehat{D}\rho(t) - \widehat{S}(t)\rho(t). \quad (3.11)$$

Let me introduce here a new probability density $d(x, t)$, such that

$$\rho(x, t) = e^{-\widehat{D}t}d(x, t). \quad (3.12)$$

Using Eqs. (3.11) and (3.12), one gets

$$-\widehat{D}e^{-\widehat{D}t}d(x, t) + e^{-\widehat{D}t}\frac{\partial}{\partial t}d(x, t) = -\widehat{D}e^{-\widehat{D}t}d(x, t) - \widehat{S}(t)e^{-\widehat{D}t}d(x, t), \quad (3.13)$$

multiply both sides with $e^{\widehat{D}t}$, then Eqn.3.13 yields

$$\frac{\partial}{\partial t}d(x, t) = -e^{\widehat{D}t}\widehat{S}(t)e^{-\widehat{D}t}d(x, t), \quad (3.14)$$

where $U(t) = e^{\widehat{D}t} \widehat{S}(t) e^{-\widehat{D}t}$. Solution of the Eqn. 3.14 is

$$d(x, t) = \exp \left[- \int_0^t dt' \widehat{U}(t') \right] d(x, 0) \quad (3.15)$$

Replacing exponential function with its series expansion $e^x = \sum_0^\infty (x^n/n!)$, and taking the average over all values of $\eta(t)$ one obtains

$$\langle d(x, t) \rangle_\eta = \left[\sum_{n=0}^{\infty} \frac{1}{(2n)!} \left\langle \left(\int_0^t dt' \widehat{U}(t') \right)^{2n} \right\rangle_\eta \right] d(x, 0). \quad (3.16)$$

Recall here that the property of noise, which describes its mean as zero and it is form as Gaussian. Therefore only even values of n remains. Average quantity $\langle \left(\int_0^t dt' \widehat{U}(t') \right)^{2n} \rangle_\eta$ decomposes into $2n!/n!2^n$ identical terms all of which contains n pairwise averages $\langle \int_0^t dt_i \widehat{U}(t_i) \int_0^t dt_j \widehat{U}(t_j) \rangle_\eta$. Using these observations Eqn. 3.16 yields

$$\langle d(x, t) \rangle_\eta = \left[\sum_{n=0}^{\infty} \frac{1}{n!} \left(\frac{1}{2} \int_0^t dt_2 \int_0^t dt_1 \langle \widehat{U}(t_1) \widehat{U}(t_2) \rangle_\eta \right)^n \right] d(x, 0). \quad (3.17)$$

Summing back the series

$$\langle d(x, t) \rangle_\eta = \exp \left[\frac{1}{2} \int_0^t dt_2 \int_0^t dt_1 \langle \widehat{U}(t_1) \widehat{U}(t_2) \rangle_\eta \right] d(x, 0). \quad (3.18)$$

Furthermore, computation of the integral $\int_0^t dt_2 \int_0^t dt_1 \langle \widehat{U}(t_1) \widehat{U}(t_2) \rangle_\eta$ yields

$$\begin{aligned} &= \int_0^t dt_2 \int_0^t dt_1 e^{\widehat{D}t_1} \widehat{S}(t_1) e^{-\widehat{D}t_1} e^{\widehat{D}t_2} \widehat{S}(t_2) e^{-\widehat{D}t_2} \\ &= \frac{1}{\gamma^2} \int_0^t dt_2 \int_0^t dt_1 \langle \eta(t_1) \eta(t_2) \rangle e^{\widehat{D}t_1} \frac{\partial}{\partial x} e^{-\widehat{D}(t_2-t_1)} \frac{\partial}{\partial x} e^{-\widehat{D}t_2} \\ &= \frac{g}{\gamma^2} \int_0^t e^{\widehat{D}t_1} \frac{\partial^2}{\partial x^2} e^{-\widehat{D}t_1}. \end{aligned} \quad (3.19)$$

Now to reach $P(x, t) = \langle \rho(x, t) \rangle_\eta$, first one should calculate

$$\frac{\partial}{\partial t} \langle d(x, t) \rangle = \frac{g}{2\gamma^2} e^{\widehat{D}t_1} \frac{\partial^2}{\partial x^2} e^{-\widehat{D}t_1} \langle d(x, t) \rangle_\eta, \quad (3.20)$$

using Eqns.3.12 and 3.20 results in

$$\frac{\partial}{\partial t} \langle \rho(x, t) \rangle_\eta = -\widehat{D} \langle \rho(x, t) \rangle_\eta + e^{-\widehat{D}t} \frac{\partial}{\partial t} \langle \rho(x, t) \rangle_\eta \quad (3.21)$$

then we reach

$$\frac{\partial}{\partial t}P(x, t) = -\widehat{D}P(x, t) + \frac{g}{2\gamma^2} \frac{\partial^2 P(x, t)}{\partial t^2}. \quad (3.22)$$

After replacing the operator \widehat{D} with its equivalent, we have the FP equation for Brownian particles inside a potential well $V(x)$ under diffusive conditions

$$\frac{\partial P(x, t)}{\partial t} = \frac{1}{\gamma} \frac{\partial}{\partial x} \left(\frac{dV(x)}{dx} P(x, t) + \frac{g}{2\gamma} \frac{\partial P(x, t)}{\partial x} \right). \quad (3.23)$$

Right hand side of the FP equation is also gives the probability current. Therefore FP equation is a continuity equation, *i.e.*, probability is conserved.

Moreover, solution of the FP equation depends on the form of the potential. The simplest form of a potential is a constant $V(x) = V$. In this case FP reduces to the heat-equation

$$\frac{\partial P(x, t)}{\partial t} = \frac{g}{2\gamma^2} \frac{\partial^2 P(x, t)}{\partial x^2}, \quad (3.24)$$

and its solution becomes

$$P(x, t) = \sqrt{\frac{1}{4\pi D}} \exp \left[-\frac{x^2}{4Dt} \right], \quad (3.25)$$

where $D = g/2\gamma^2$.

Chapter 4

Original Work

4.1 Strong Frequency Dependence in Over-damped Systems

Strong frequency dependence is a rare phenomenon in over-damped or diffusive environments. The existence of it, such as stochastic resonance, indicates interesting underlying dynamics. In our work, we encountered an example of such phenomenon which occurs in the Brownian motion of an over-damped particle under the effect of periodically oscillating retarded force that emanates from the boundaries. We found that, the amplitude of the expectation value of position has significant frequency dependence which is not how typical resonance behaves. We model this motion with a Fokker-Planck equation. This problem appeared when we study the Brownian motion of shock profile of TASEP. In this section I will first describe the details of our Fokker-Planck analysis. Then I will discuss how this model is relevant to the motion of shock profile.

In diffusive environment, periodic forces cannot build growing oscillations. System's response to such forces is monotonous. We suggest an over-damped system which gives an oscillating frequency response to a position dependent effective force. Such system are realizable, for Brownian motion under the influence of

retarded effects coming from the boundaries.

As described in the previous chapter, Fokker-Planck (FP) equation [87, 88, 89, 90, 91] gives the time dependence of the probability distribution $P(x, t)$ of the position of a particle in a over-damped system:

$$\frac{\partial P}{\partial t} = \frac{\partial}{\partial x} \left[-\gamma P \left(-\frac{\partial V}{\partial x} + F_{ret} \right) + D \frac{\partial P}{\partial x} \right] \quad (4.1)$$

where γ and D are drift and diffusion constants respectively. In our model, potential energy $V = V(x)$ is time-independent. And the force F_{ret} is retarded and emanates from the boundaries. It is sinusoidally time and position dependent.

There are significant amount of work dedicated to the behavior of probability P under the influence of different potentials. Analytical solutions can be offered for simple potential forms. The equation may be treated as Schrödinger equation with imaginary time. Its solutions have relaxational behavior in time. The behavior is the consequence of absence of inertia (no force is proportional to dx^2/dt^2 or memory in the system, *i.e.*, the probability of the position of the particle in the future time $t + dt$ depends only on the probability on current time t). However, in our case we can get an amplified response from the memoryless system due to the matching of wavelength and the length of the interval between the boundaries.

Other over-damped phenomena of amplified response (non-monotonous response) are also present in the literature. For instance in Brownian motors, a Brownian particle moves in a ratchet type independent potential and a sinusoidal force drives the particle over the less steep barrier [92]. The motion is asymmetric either due to the form of the static potential or due to the time-dependent forces. Moreover, in vibrational resonance [93] a high-frequency drive may effectively average over the portions of the potential. The length scale of averaging depends on the drive. Also, the transport properties of the system depend strongly on the drive. The force can be of a superposition of sinusoidal or rectangular functions, which may lead to interesting non-linear effects for certain combination of frequencies [94]. For further information about these and other similar systems, review by Hänggi and Marchesoni is recommended [95].

Finally there is the stochastic resonance [96, 97, 98, 99, 100, 101], which is the phenomenon related to the motion of Brownian particle inside a double-well potential, under the effects of random diffusive force and a sinusoidal force. In this system, for an optimal value of the magnitude of the random force, transitions between the walls of the potential amplifies in synchronism with the sinusoidal drive. Corresponding FP equation was solved by Jung and Hänggi [97]. They demonstrated that the time auto-correlation function of this system sustains undamped oscillations. In this case, resonance means the amplified response of the switching between the wells at a certain value of the magnitude of the random force. A wide variety of systems can be modeled this way, such as seasonal changes on population systems [102], the dependence of stock prices on periodic information flow [103], and many other biological phenomena [104, 105]

All of these phenomena include static multiple potential wells and position independent sinusoidal forces. However, our model incorporates a static mostly flat (quadratic at the boundary regions and flat in between) potential and a sinusoidal retarded force that emanates from the boundaries. There are not many studies of effect of such force field in the literature, *i.e.*, force field which propagates from the boundaries with a finite velocity. Relevant works are analysis of a diffusive system in which particles are introduced to the system from a single boundary and annihilate each other upon contact [106]. Also there is an another system, with a position dependent sinusoidal force coupled to a bath of oscillators, acting as a random force was derived the effective force of this Hamiltonian system [107].

The existence of propagating effects within a memoryless, over-damped system may seem contradictory. However, mechanisms that drives the diffusion dynamics can be different than the mechanisms that generates the effective force. For instance in TASEP, diffusion of the shock front in the bulk is effected from the change in the boundaries after a delay. Thus we claim shock motion of TASEP is a discrete realization of the aforementioned FP system.

4.1.1 Analysis and Discussions

4.1.1.1 Fokker-Planck Equation

In our analysis, our static potential $V(x)$ has the form

$$V(x) = \begin{cases} 0 & \text{if } |x| < \frac{L}{2} \\ V_0(|x| - L/2)^2/x_0^2 & \text{otherwise.} \end{cases} \quad (4.2)$$

The quadratic structure relaxes the boundaries $\pm L/2$ with a range length x_0 . Moreover, we have a time dependent force which is emanated simultaneously from the boundaries and acts on the particle. The force is retarded in time, *i.e.*, it reaches the particle with a constant velocity v after a delay proportional to its distance to the boundaries.

$$\begin{aligned} F_{ret}(x, t) &= F_0 \sin \left[\omega \left(t - \frac{L/2 + x}{v} \right) \right] \\ &\quad + F_0 \sin \left[\omega \left(t - \frac{L/2 - x}{v} \right) \right] \\ &= 2F_0 \cos \frac{\omega x}{v} \sin \left[\omega \left(t - \frac{L}{2v} \right) \right]. \end{aligned} \quad (4.3)$$

Although the magnitude F_0 of the force is constant, its effects display strong frequency dependence. Eqn. 4.3 indicates that the effects of this retarded force results in a position and frequency dependent amplitude ($2F_0 \cos(x\omega/v)$). Our analysis shows that this force depends on how the wavelength compares to the system size L .

Our FP equation in scaled form is

$$\begin{aligned} \frac{\partial P(z, \theta)}{\partial \theta} &= \Gamma \frac{\partial}{\partial z} \left[P \frac{d\tilde{V}(z)}{dz} - \epsilon \cos(2\pi z/\lambda) \sin(\theta) \right] \\ &\quad + \bar{D} \frac{\partial^2 P}{\partial z^2} \end{aligned} \quad (4.4)$$

where we have used the dimensionless quantities in Table 4.1 with unitless potential:

$$\tilde{V}(z) = \begin{cases} 0 & \text{if } |z| < \frac{1}{2} \\ (|z| - 1/2)^2 L^2/x_0^2 & \text{otherwise.} \end{cases}$$

Parameter λ represents the wavelength of the time-dependent force relative to the unitless distance variable z . It is also proportional to the period of oscillation: $\tau = 2\pi/\omega = \lambda L/v$.

We have provided numerical results of Eqn. 4.4 for solution of $P(z, \theta)$ on a mesh of 256 points in the z direction. The length of interval of z is L ($|x| < L/2$) plus two boundary regions of size $3x_o$ wide each. Then, the equation is integrated with respect to time variable θ . The step size of the integration is $\Delta\theta/(\Delta z)^2 \leq 0.1$. The integration is started with an arbitrary initial condition at $\theta = 0$ and is carried out until there is no significant change in $P(z, \theta)$. Integral converged in ten repetitions for the period of $\theta = 2\pi$.

Expectation value of position as a function of θ is calculated as:

$$\bar{z}(\theta) = \int_{-\infty}^{\infty} dz z P(z, \theta).$$

And, fundamental Fourier coefficients that parametrizes the size of the oscillations are calculated as :

$$\begin{aligned} C &= \frac{1}{2\pi} \int_0^{2\pi} \bar{z}(\theta) \cos(\theta) d\theta \\ S &= \frac{1}{2\pi} \int_0^{2\pi} \bar{z}(\theta) \sin(\theta) d\theta. \end{aligned} \quad (4.5)$$

In Fig. 4.1, it can be seen that the response of the system has non-monotonous frequency dependence. When the boundaries becomes sharper, the amplitude of oscillations grow as the boundary to bulk ratio x_o/L decreases. More oscillations of probability density fit inside of a wider boundary. Moreover, wider boundary diminishes the variations in \bar{z} and the features of the plots expand as it gets wider. Latter signals longer wavelengths for which the response reaches to its asymptotic value. Here also observe that S component of the response dominates for smaller x_o/L ratio. In our calculations we choose the size of ϵ , so that magnitude of response becomes comparable to that obtained from the Monte Carlo analysis.

The matching of wavelength with $L + 6x_o$ (effective length of diffusion plus the boundary region) correspond to the extrema of the response. In Fig. 4.2 we show

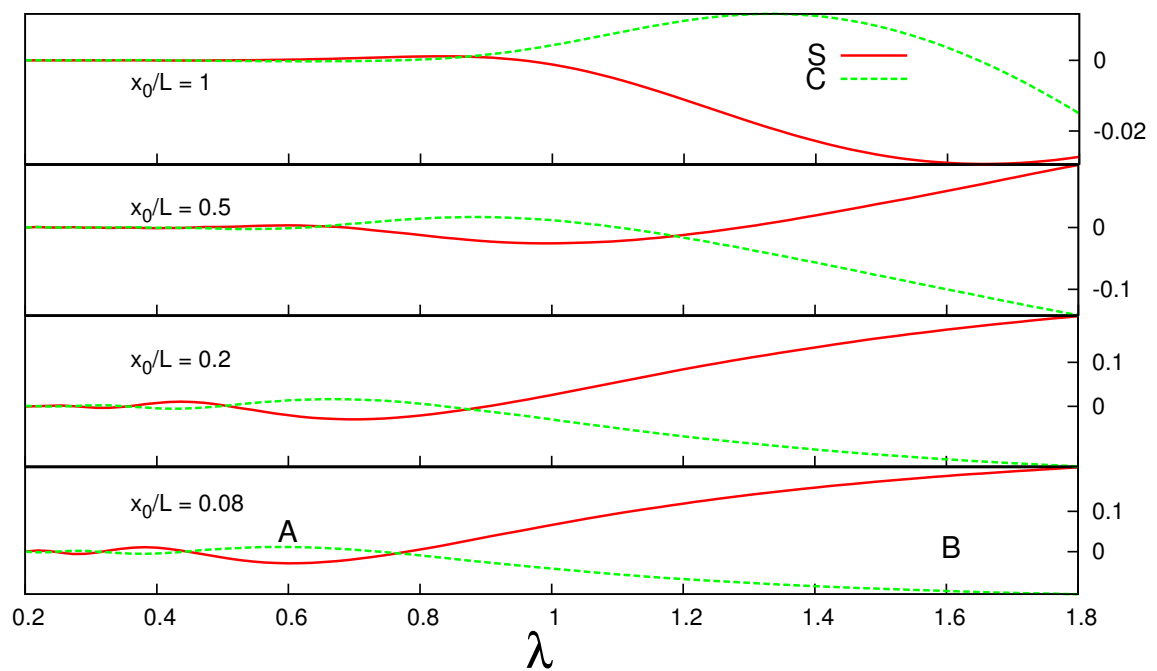


Figure 4.1: First Fourier components that give the magnitude of the oscillatory response (as the expectation value of the position) of the system as a function of wavelength. Each plot corresponds to different values of boundary smoothness x_0/L . Dotted line corresponds to the cosine (C) or out of phase component and continuous line corresponds to the sine (S) or in phase component. Notice here that the scales of the plots are not equal.

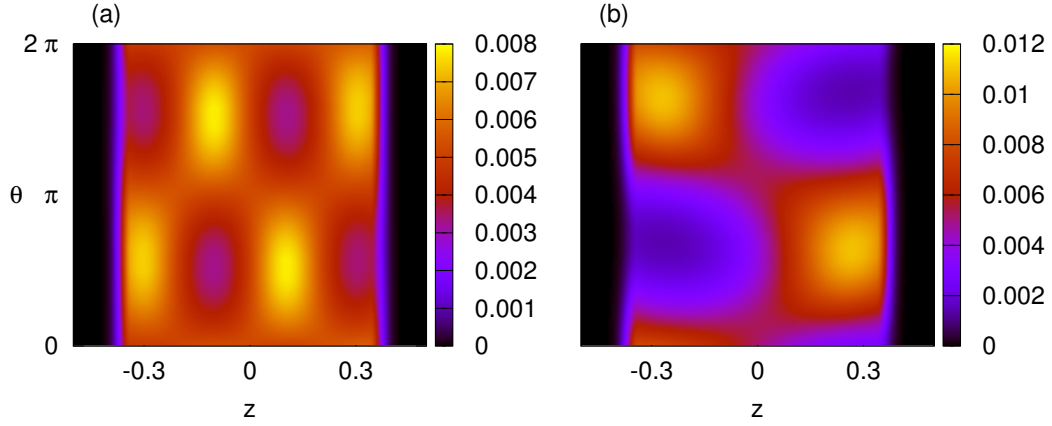


Figure 4.2: The probability densities of marked points in Fig. 4.1. (a) Point **A** ($\lambda = 0.6$) accounts to consecutive dark and light patterns along the x-axis, which indicates standing waves of two wavelengths that fits to the lattice size. (b) Point **B** ($\lambda = 1.6$) accounts to only one wavelength.

that the probability densities corresponding to points *A* and *B* in Fig. 4.1. In both of the plots (a) and (b) probability densities increase with z for $\theta \sim \pi/4$ and $z \sim 0$. Parity of the number of the maxima present in the response effects position expectation value. If there are even number of maxima, position expectation value is negative and if there are odd number of maxima, then the value is positive. The graph shows oscillations as a function of wavelength. In case of more wavelength fitting into the system (small λ) the change in z becomes less apparent.

Dimensionless Quantities	
$\theta = \omega(t - L/(2v))$	$\Gamma = \gamma V_0/(\omega L^2)$
$z = x/L$	$\epsilon = 2F_0L/V_0$
$\lambda = 2\pi v/(\omega L)$	$\bar{D} = D/(\omega L^2)$

Table 4.1: Dimensionless quantities that are used in scaling the Fokker-Planck equation.

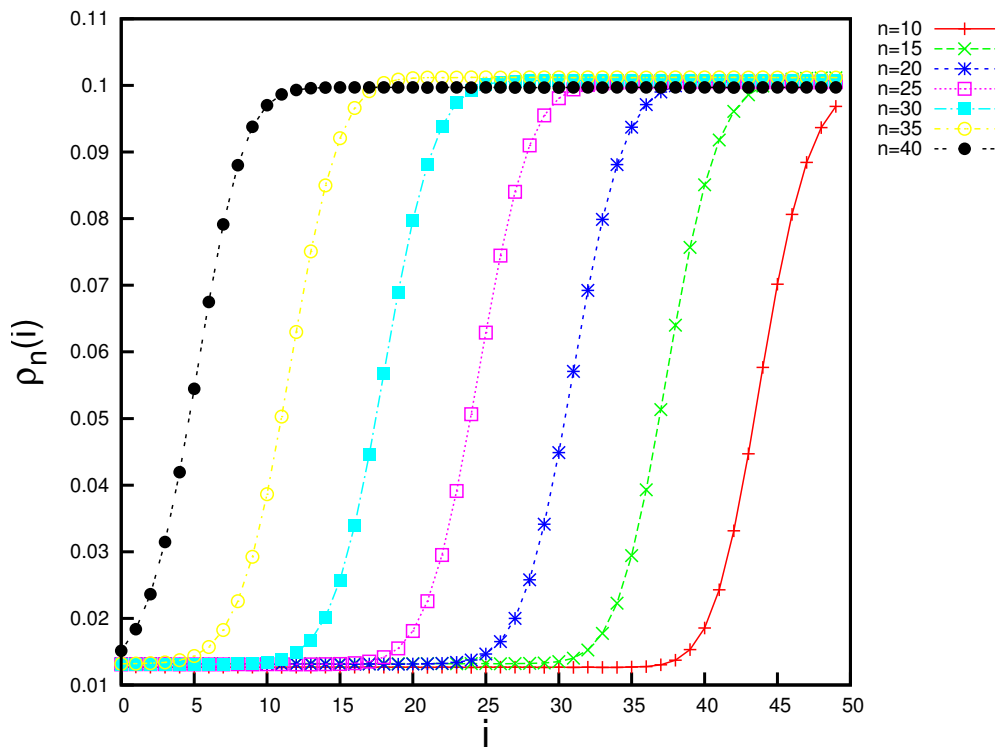


Figure 4.3: Shock profile distributions for various numbers of particle number.

4.1.1.2 TASEP

As was discussed in previous chapters, TASEP with one class of particles can be defined on a one-dimensional lattice with open boundaries. And these systems support shock profiles of densities. We claim that the motion of a shock profile of TASEP under periodical boundary conditions is a discrete realization of our FP model.

Majority of the studies in literature have been focused on TASEP with time-independent boundary rates. However, there are some recent studies on TASEP with time-dependent rates. For instance Popkov *et al.*, studied TASEP as a vehicular traffic model under alternately changing red and green traffic lights [108]. Also Basu *et al.* studied frequency dependent modality on another transport system [109].

As we have discussed in Chapter 3, on the phase transition line between high and low density phases ($\alpha = \beta \leq 1/2$), the system support macroscopic objects, namely shock profiles. In the MC simulations they correspond to the occupation statistics of states for associated particle number. Microscopically they are the segregated states where occupied sites are accumulated to the exit boundary and vacancies accumulate to the entrance boundary. It is reported that these profiles do a random walk inside the lattice [36]. We have chosen to study shock structures macroscopically, since macroscopic structures also display Brownian motion characteristics, along with their easier to measure statistics [36]. Fig. 4.3 displays these profiles for a lattice of size $N = 50$. Each profile corresponds to a different particle number n . Moreover, the flat part of Fig. 4.5 shows that all the particle numbers in that region are equally likely to be found in the lattice. This result suggests that the shock profiles do a random. The random walk is constrained by the boundaries. The mechanism of constraint works in the following way: If the profile gets too close to the entrance boundary, *i.e.*, lattice get very crowded, particles can enter the system at a smaller rate. And eventually particle number decreases and the profile “feels” it is pushed to the middle of the lattice. Or else, if the profile gets too close to the exit boundary, *i.e.*, lattice get very sparse, less particles leave the system and new particles enter the lattice. Particle number increase, which translates to the pulling of the profile to the midst of the lattice. This mechanism is the cause of non-flat regions around boundaries in the Fig. 4.5.

The above motion can be interpreted as a random walk inside an effective potential of $V(x)$, the form of which is the same with the form of associated free-energy functional proposed by Arndt *et al* [80]. It is also the form of our static potential in FP analysis.

In our work, we report the effect of sinusoidally varying boundary rates to the TASEP with single class of particles. Monte Carlo simulation was used in the rest of the studies in this chapter. Perturbation causes the frequency of particle entry or exit rate to change. Therefore, the change in the boundary rates causes a change in the particle number. This change is conveyed to the shock position after a delay. It can be see in Fig. 4.4 that the position of the profile is linearly

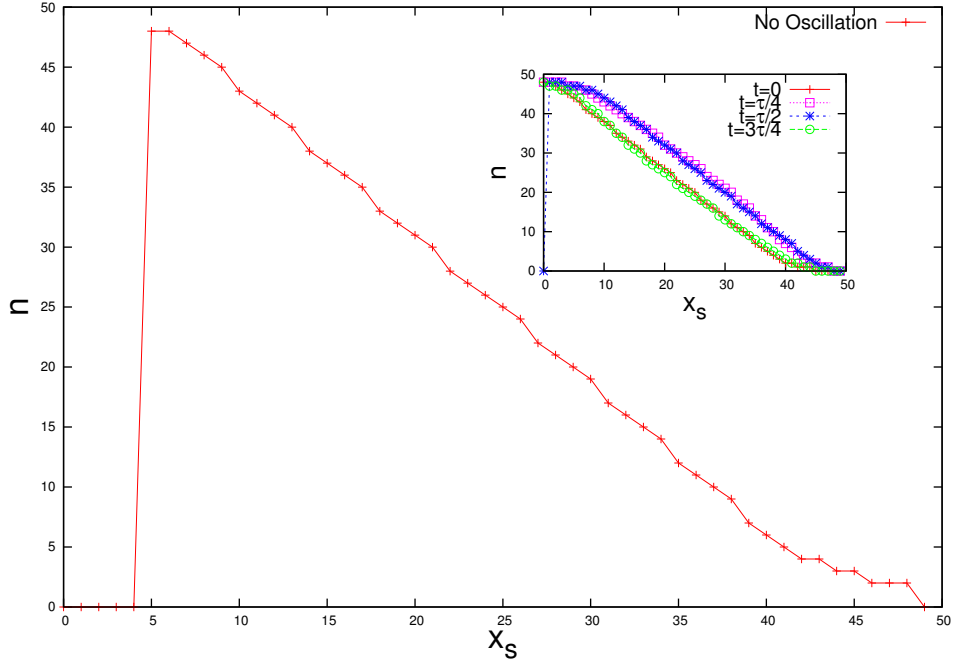


Figure 4.4: The linear relationships between particle number n and shock position x_s for the profiles in Fig. 4.3. The shock position x_s is defined as the lattice position at which the density $\rho_n(i)$ corresponds to the midpoint of the profile. The inset displays the relationship when boundary conditions change sinusoidally with period τ as discussed in the text. Here $N = 50$ and $\tau = 120$.

dependent on particle number. By exploiting this fact, we track the particle number instead of shock position.

Figure 4.6 demonstrates the effect of periodic pulse type of perturbation to the particle entry rate on $P(n)$ (given in Fig. 4.6). We defined this perturbation as follows: We increase the entry rate (on the order of 10 times of the usual rate, *i.e.*, $\alpha = 5$) very much for a time of duration 0.1τ ; then we take the response statistics for during a period of length τ . While reporting, in order to make the effects more visible time averaged values of $\langle \bar{P}(n) \rangle_\tau$ are subtracted from $P(n)$. We divide the period into four quarters. In the first quarter the pulse causes an increase in particle number, which tells us that the probability of finding the shock profile near the entrance boundary is increased. The bump in the particle number relaxes to its original state ($P(n) - \langle \bar{P}(n) \rangle_\tau = 0$). However, in the

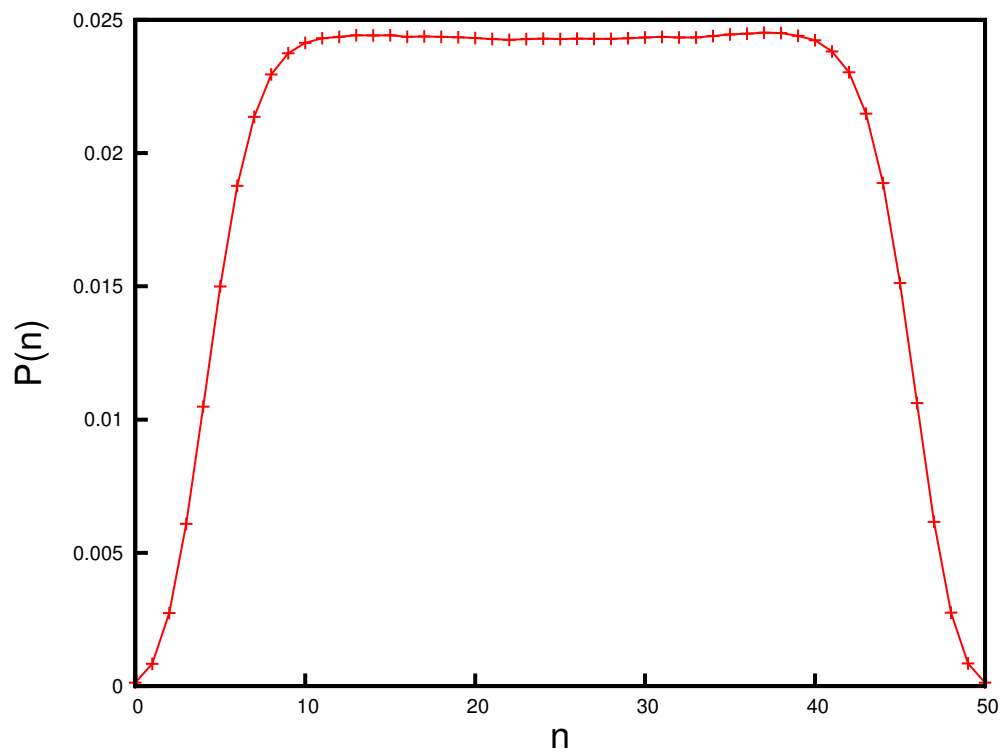


Figure 4.5: Probability distribution $P(n)$ of particle number n ., for a lattice size of $N = 50$ and $\alpha = \beta = 0.1$.

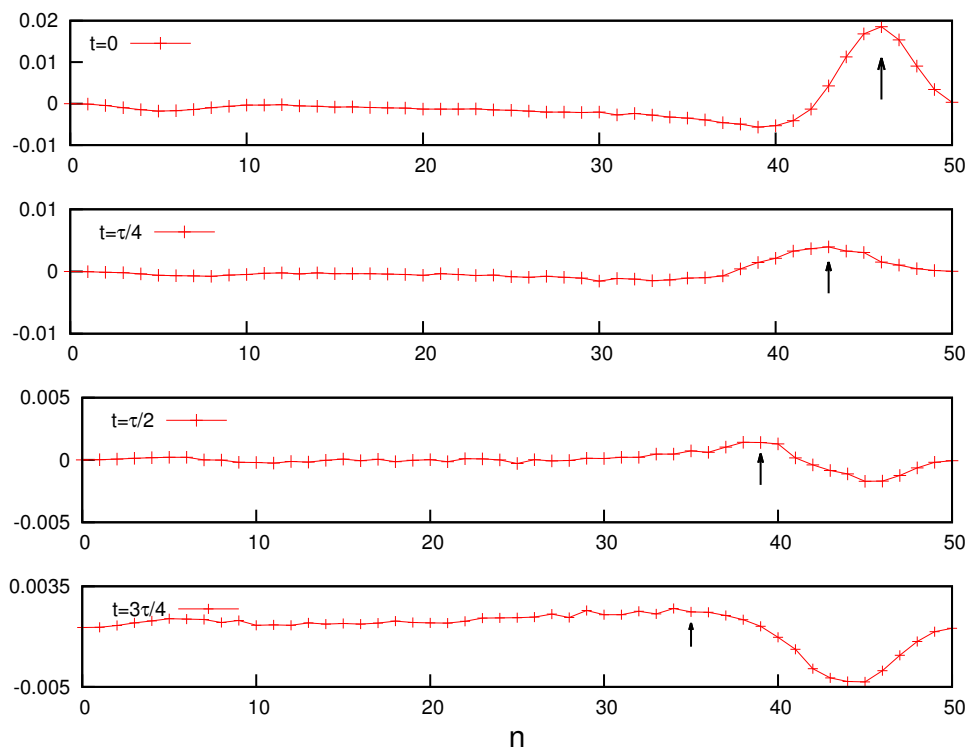


Figure 4.6: Response of the probability distribution function $P(n)$ to a pulse type perturbation to the entrance rate. The arrows shows the maxima of the curves. See text for the details.

second half of the motion retarded response is apparent. Higher values of the particle number diminishes (pits of the distribution) yet lower values of particle numbers are increased as a whole (notice overall slight increase in smaller particle numbers). This tells us that shock profile is found most likely around the entrance boundary and then walk inside of the lattice. This retarded effect on the motion justifies our association of this model with Eqn. 4.1. However, response of the TASEP system (Fig. 4.8 and Fig 4.7) is not as clean as the response of the FP system (Fig. 4.1 and Fig 4.2). This problem is due to the diminishing of effective force away from the boundaries as a result of stronger damping of TASEP.

I will now describe our study of sinusoidal perturbations to the system. I have described the kinetic Monte Carlo method in the previous chapter. The method needs pre-determined transition rates given as an input to the algorithm. In this model, we have time dependent transition rates at the boundaries and static rates elsewhere. The time-dependent rates are of the form:

$$\beta = \beta_o - \Delta\beta \sin(\omega t), \quad (4.6)$$

and

$$\alpha = \alpha_o + \Delta\alpha \sin(\omega t). \quad (4.7)$$

These rates are assumed to be constant during a time step Δt , since $\Delta t \ll 2\pi/\omega = \tau$. Time t_n in n th continuous time step is calculated as $t_n = (t_{n-1} + \Delta t) \bmod \tau$. Here τ is the period of oscillation. We carried out the simulation for 10^6 Monte Carlo steps (MCSs). We define a MCS as N^2 changes in the lattice of size N .

We choose a small lattice size to simulate, since we have observed that boundary effects weaken substantially inside the lattice. Also we choose small values of α and β , as this choice corresponds wider range of random walk. Therefore, we take lattice size as $N = 50$, and the $\alpha_o = \beta_o = 0.1$. We perturbed the system around this point with a significant amplitude such as $\beta = 0.1 - 0.099 \sin(\omega t)$ and $\alpha = 0.1 + 0.099 \sin(\omega t)$. This perturbation drives the system between high and low density phases. Fig. 4.7 shows the probability density $\rho(n, t)$ of finding n particles in the system at time t . The results qualitatively agree with the FP results. However, note here that in Fig. 4.7, the time average of the density was subtracted from $\rho(n, t)$ to magnify its time-dependence. Also note that the scales

in Fig. 4.7 are with respect to the variable t , while those in Fig. 4.2 are with respect to θ , which contains a phase shift.

Moreover, we choose corresponding FP parameters so that these analysis become compatible with each other. For instance, we choose diffusion constant of FP equation to be $D = \Delta$, where $\Delta = 2\alpha(1 - \alpha)/(1 - 2\alpha)$ is known exactly ???. For $\alpha_0 = \beta_0 = 0.1$ this yields the value $D = 0.225$. Also, in FP analysis boundary width to lattice length ratio is taken as $x_o/L = 0.08$, since we have observed in MC analysis that there is atypical behavior within two lattice sites to the boundaries. (Note here that we exclude this problematic region when drawing Fig. 4.7.)

Similar to the FP analysis we measured the fundamental components of the response of the system:

$$\begin{aligned} C &= \frac{1}{\tau} \sum_0^{\tau} \bar{n}(t) \cos(2\pi t/\tau) \\ S &= \frac{1}{\tau} \sum_0^{\tau} \bar{n}(t) \sin(2\pi t/\tau) \end{aligned} \quad (4.8)$$

where

$$\bar{n}(t) = \sum_n \rho(n, t)n. \quad (4.9)$$

Fig. 4.8 shows the C and S components of the response. It is apparent that oscillations are not as clear as the ones obtained from the FP analysis. We attribute this to the weakening of the effective force away from the boundaries. This damps the effect in higher frequencies. However, the force is still effective enough to cause frequency dependent response.

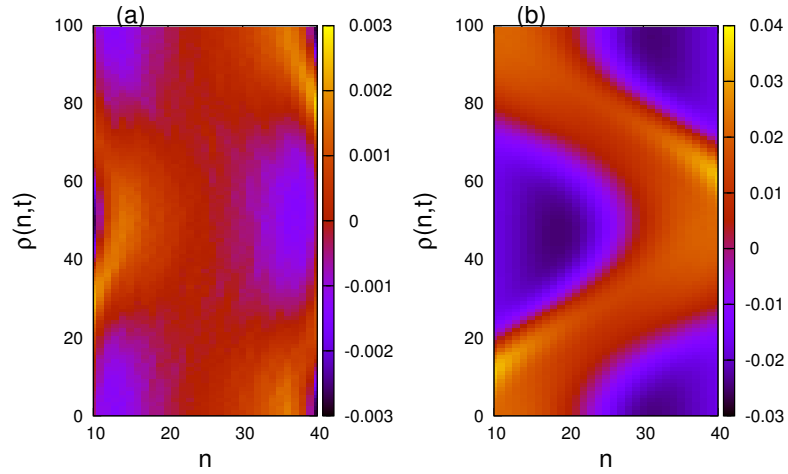


Figure 4.7: Change in probability density $\rho(n,t)$ from its time average. Point a and b are marked in Fig. 4.2. (a) Point a ($\tau = 140$) accounts to two wavelengths. (b) Point b ($\tau = 700$) accounts to one wavelength of the system. Simulations are carried out for $N = 50$ and different periods calculated over 10^6 MCS.

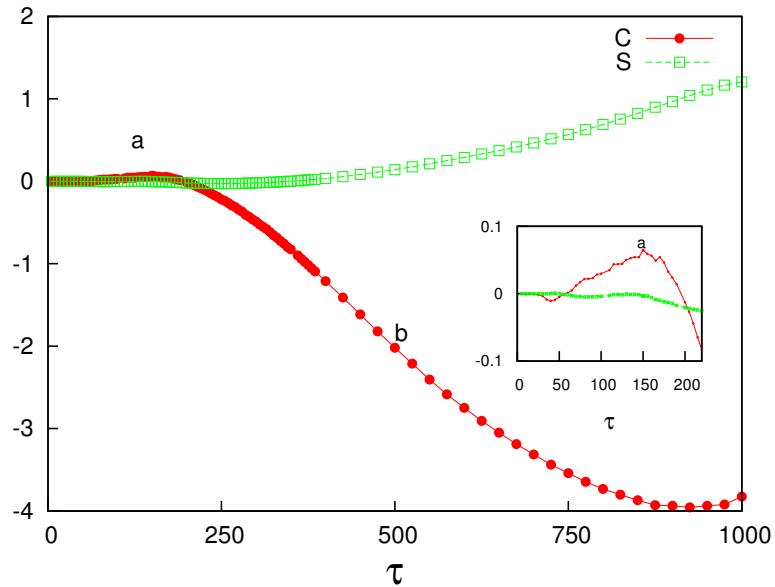


Figure 4.8: Fundamental components (C and S in Eqn. 4.8) with respect to different period values. It is apparent that the response of the system has resonance like structure. Points a and b correspond to the density distributions in FIG. 4.7. Inset shows there is also sinusoidal behavior present for smaller values of τ .

4.2 Dynamical Phase Transitions in TASEP

This section describes our MC analysis of TASEP with two classes of particles under periodically oscillating boundary conditions. We oscillate the boundary rates around a phase transition point. We show that depending on the frequency of the perturbation, system's response changes significantly. Furthermore, we identify a dynamical phase transition between a symmetric response and a near-symmetric response. The transition is abrupt, it is a function of frequency and it is independent of magnitude of the perturbation.

As we have discussed in Chapter 3, the model has four phases, half of which are symmetric and the other half is asymmetric. The symmetric phases are power law (P) and low density (L) phases. And the asymmetric phases are a tiny regime (TR) and high density-low density phase. In the symmetric phases both of the particles are at the same state, but in the asymmetric phases even though the parameters are symmetric for both of the particles they are not in the same state, *i.e.*, spontaneous symmetry breaking occurs. Fig. 4.9 displays joint probability density functions $\rho(n_1, n_2)$ for some of the parameters which are relevant to our work. These points are chosen either from the TR phase or they are in close proximity of this phase. The TR phase is composed of superpositions of shock

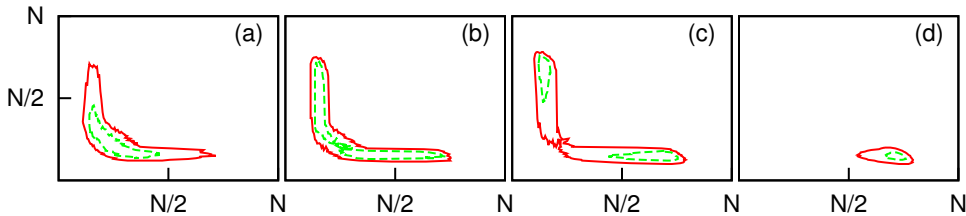


Figure 4.9: Joint probability density functions $p(n_1, n_2)$ for various parameters under constant BC. Exit rates for the plot (a) are $\beta_1 = \beta_2 = 0.285$, for the plot (b) are $\beta_1 = \beta_2 = 0.275$, and for the plot (c) are $\beta_1 = \beta_2 = 0.265$, and for the plot (d) they are asymmetric as $\beta_1 = 0.265$ and $\beta_2 = 0.285$. For all of the graphs the rest of the rates are equal to 1.

profiles. Fig. 4.10 shows these profiles. Each of the plot corresponds to the density distribution of first class of particles only, provided that $n_1 > n_2$. This condition implies limiting the average to the one leg (lower half of $n_1 = n_2$ line) of

the boomerang shaped probability distribution. In agreement with our previous model, motion of shock profiles under periodic boundary conditions is composed of two different features. One of them is the diffusive motion inside an effective force and the other one is the motion under an effective force that is created by the manipulation of boundary conditions. The latter has a retarded effect on the position of the shock. We have observed interesting phenomena through the interplay of these two features such as strong frequency dependence and hysteresis in the density function of the system. This hysteresis behavior was observed in similar systems [110]. However, in our system hysteresis appears abruptly when perturbation frequency is lowered. We associate these phenomena with a typical velocity within the system.

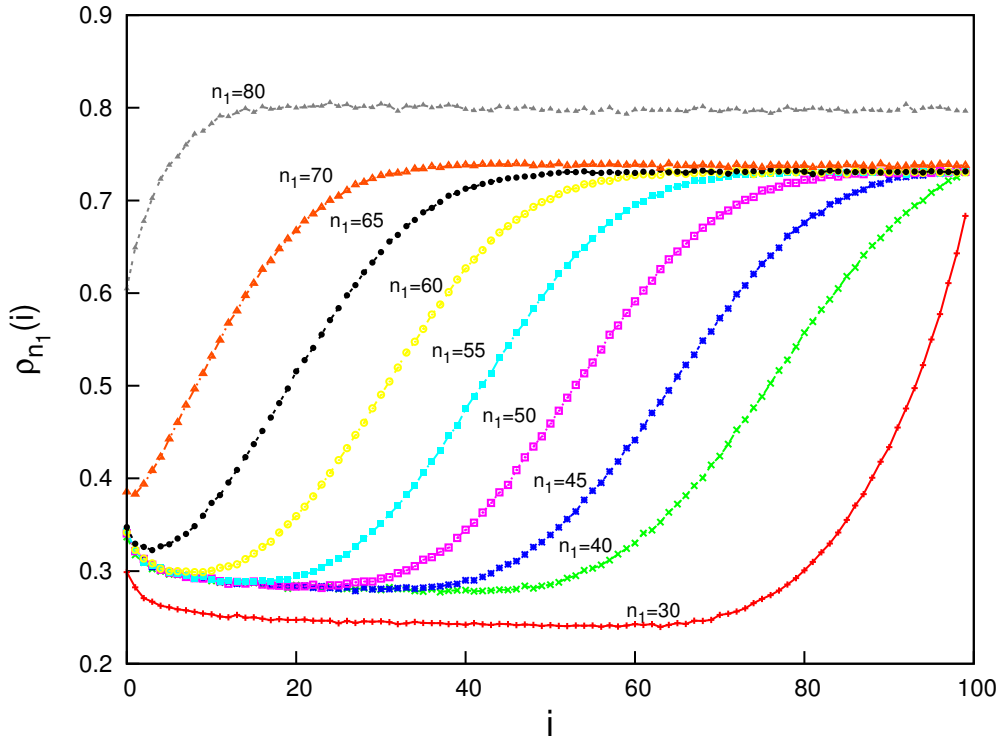


Figure 4.10: Various shock profiles in a system size of $N = 100$. Time-independent boundary rates are $\alpha_1 = \alpha_2 = 1$ and $\beta = 0.2675$.

4.2.1 TASEP under Periodically Driven BC

The kinetic Monte Carlo analysis of this work shares the basics with our previous study. Apart from the introduction of the second class particles, differences lie on the which and how rates are oscillated. In this model, we only oscillate the exit boundary rates and take all other rates to be equal to 1. The exit rates oscillate as

$$\begin{aligned}\beta_1 &= \beta_o - \Delta\beta s(t) \\ \beta_2 &= \beta_o + \Delta\beta s(t)\end{aligned}$$

where $s(t) = \text{sgn}[\sin(2\pi t/\tau)]$. Here τ is the period of oscillation, $\Delta\beta$ is the magnitude of oscillation and $\beta_1 = \beta_2 = \beta_o$ is the anchor point we oscillate the boundaries around. In order the remain in the TR phase we have taken $\beta_o = 0.275$ and $\Delta\beta = 0.1$. Each MC simulation is for 10^5 MCS. We calculated the period dependent averages by obtaining time dependent averages within each period and them averaged over the periods.

4.2.2 Variations in the character of Frequency Dependence

We oscillate the boundary rates in a way that we can break the symmetry between the two classes of particles. Our anchor point is in TR, since in this parameter regime, system supports the widest range of random walks of shock fronts.

Before going further let me share some observations with you. For instance, for very high frequencies, effective boundary rates equate the anchor value and system remains in the unperturbed state. On the other hand for very low frequencies system flows from one asymmetric boundary state to the other. We utilize joint probability density distribution to capture the characteristics of responses. Depending on the frequency, these characteristics vary significantly. The results for a system of size $N = 200$, with respect to different frequencies are in Fig. 4.11. It can be observed that the boomerang-shaped profile (such as the ones in Fig. 4.9)

can appear and disappear as a function of frequency. This shape of the density distribution is preserved for high-frequencies of oscillation. However, this distribution is not static. It is slightly displaced in response to the perturbation. We name these states as “near-symmetric” states. Their joint density functions do not preserve the exact symmetry between two classes of particles due to the displacement. However, they maintain their shape during a perturbation cycle.

Nonetheless, the shape varies at different frequencies. It can be of the form which resembles the shapes in Fig. 4.9. However, the shape corresponds to $\tau = 300$ is not in Fig. 4.9. To reach this kind of shape, one needs to go for higher values of β (deeper into the L phase), which is not in the parameter range of oscillations. This signals a resonance-like response of the system, *i.e.*, by oscillating the boundary parameters one can drive the density fluctuations much higher than it can be obtained from the static values in the same range. By further changing the frequency the boomerang shape is regained.

We quantify the response behavior by introducing a new variable. We start by dividing a period into 100 time intervals as $t_i = i\tau/100$ where i is i th interval $0 \leq i \leq 100$. And $\langle n_1 \rangle_{t_i}$ and $\langle n_2 \rangle_{t_i}$ are the expectation values of particle numbers at time t_i .

$$\begin{aligned}\langle n_1^m \rangle_{t_i} &= \sum_{n_1, n_2} n_1^m p(n_1, n_2, t_i) \\ \langle n_2^m \rangle_{t_i} &= \sum_{n_1, n_2} n_2^m p(n_1, n_2, t_i) \\ \Delta_1^2(t_i) &= \langle n_1^2 \rangle_{t_i} - \langle n_1 \rangle_{t_i}^2 \\ \Delta_2^2(t_i) &= \langle n_2^2 \rangle_{t_i} - \langle n_2 \rangle_{t_i}^2\end{aligned}$$

We define the new variable “average spread” as

$$\bar{\Delta} = \sqrt{\frac{\sum_i (\Delta_1^2(t_i) + \Delta_2^2(t_i))}{100}}$$

The parameter $\bar{\Delta}$ gives the average fluctuation value in number of particles during a period. Figure 4.12 displays $\bar{\Delta}$ as a function of period. The extrema of the graph indicate resonance-like behavior. These points are identified with letters $A - E$, each of which corresponds to the distributions in Fig. 4.1. For instance,

for point A density is similar to L phase with some tail into symmetry broken phase ($\tau = 140$) or for point B ($\tau = 190$) the shape is very similar to the boomerang-shape of the symmetric case. The density shape corresponding to point C ($\tau = 300$) has the shape of deep L phase discussed above. Point D ($\tau = 610$) corresponds to a near-symmetric phase with displacements. Finally for point E ($\tau = 2900$) and the points beyond, system stays in the symmetry broken phases. In these low frequencies, hysteresis structure emerges abruptly.

Fig. 4.13 displays the effect of magnitude of oscillation on the spread parameter. It is apparent that the structure of the response remains the same, and it is also apparent that it depends on the amplitude ($\Delta\beta$). At higher frequencies, decrease in the amplitude results in decrease in the variation of the spread. However, at lower frequencies it gets harder to push the system to the asymmetric states. Therefore, it takes longer times for spread to subside. Figure 4.14 shows the results of the response with respect to the change in lattice size. The figure indicates that characteristic times of the system are scaled by N . This is already expected, since there is a typical velocity of the system. Yet, the response extrema are not simply scaled by N since they may be affected by the boundary regions.

Fig. 4.15 shows the hysteresis behavior as a function of τ . The structures are joint probability distribution functions drawn with respect to expectation values of particle number. The area A that one wing of the hysteresis covers is

$$A = \sum_{t_i} \langle n_2 \rangle_{t_i} \Delta \langle n_1 \rangle_{t_i}.$$

Here $\Delta \langle n_1 \rangle_{t_i} = \langle n_1 \rangle_{t_i} - \langle n_1 \rangle_{t_{i-1}}$, and the summation is on one wing. Figure 4.16 displays that hysteresis exists for all frequencies yet large-scale hysteresis appears when period becomes at the order of $\tau \sim 5N$. These results are independent of the amplitude or the lattice size. This limit is the starting point of the large scale motion of the probability density (in the A vs τ). This motion signals system is no more in a near-symmetric state. The typical velocity of the system can be estimated as $\tau/N \sim 0.2$. Existence of it implies that faster frequencies cannot induce large scale hysteresis. The inset to Fig. 4.16 displays that the

starting point of the large scale motion has some structure. This point is the the dynamical phase transition point, where tuning parameter is the frequency.

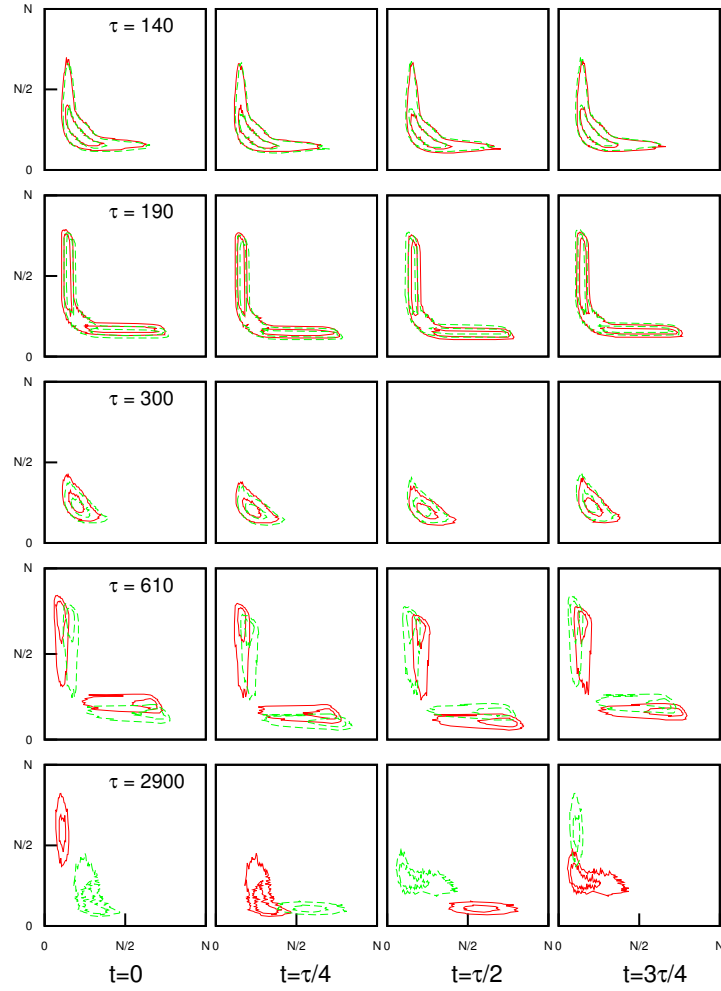


Figure 4.11: Time dependence of the joint density distribution $\rho(n_1, n_2)$ corresponding to the marked points in Fig. 4.12. In each plot, the density at time t as well as density at $t + \tau/4$ (dashed lines) are drawn together to display the motion or the change of shape. Here $N = 200$ and $\Delta\beta = 0.1$.

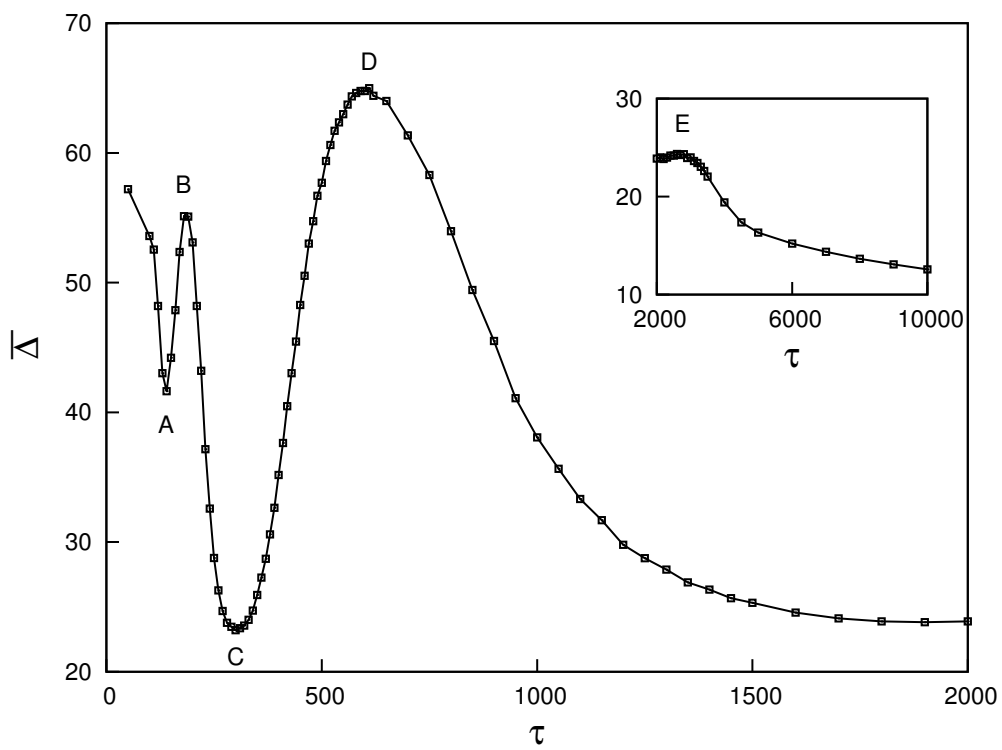


Figure 4.12: Average density spread ($\bar{\Delta}$) graph with respect to different period values. Inset shows the average spread for higher values of period. Interesting points are labeled with letters (see details in text). Density distribution for these points are given in Fig. 4.11.

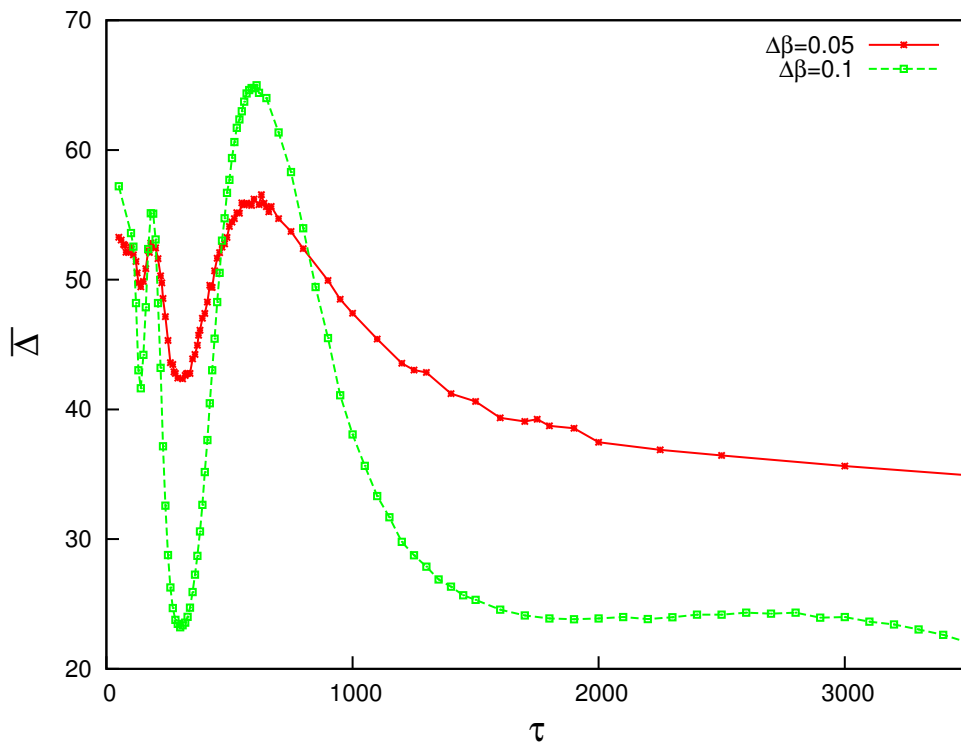


Figure 4.13: Average density spread ($\bar{\Delta}$) responses of the system for different magnitudes of perturbation, $\Delta\beta \in 0.05, 0.1$. It is apparent that the extrema of the response is independent of the size of the periodic drive.

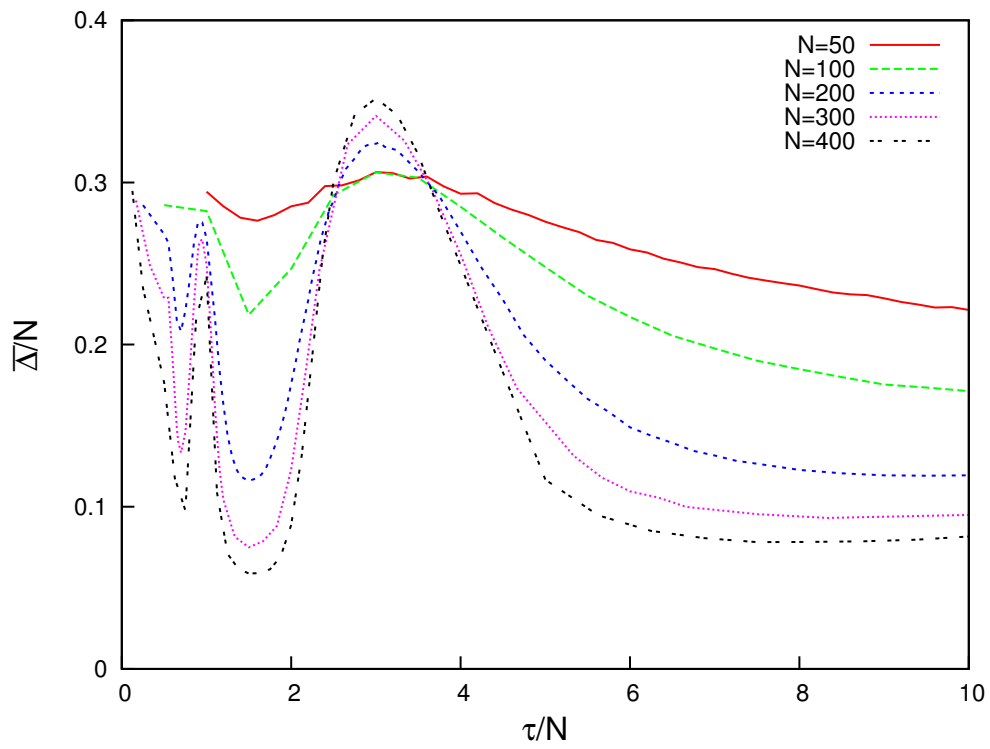


Figure 4.14: Average density spread ($\bar{\Delta}$) with respect to oscillation period τ for various values of lattice sizes. Both axes are scaled by N .

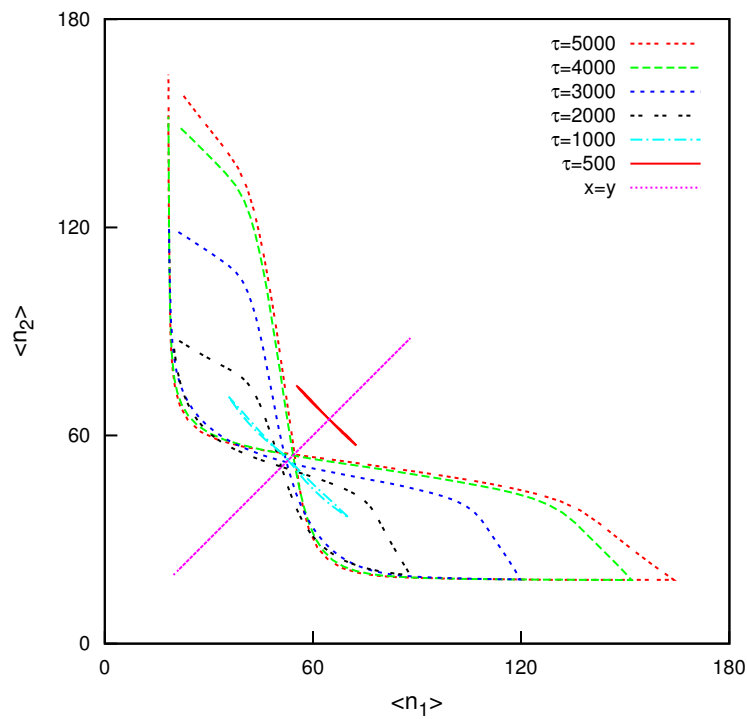


Figure 4.15: Hysteresis plots as a function of different periods of oscillation (τ). They are formed by following the trajectory of $\langle n_2 \rangle_{t_i}$ vs $\langle n_1 \rangle_{t_i}$ for values of t_i within a period. The trajectory reaches its limiting forms (two of them are present) starting from $\tau \geq 5000$ and below $\tau \leq 500$.

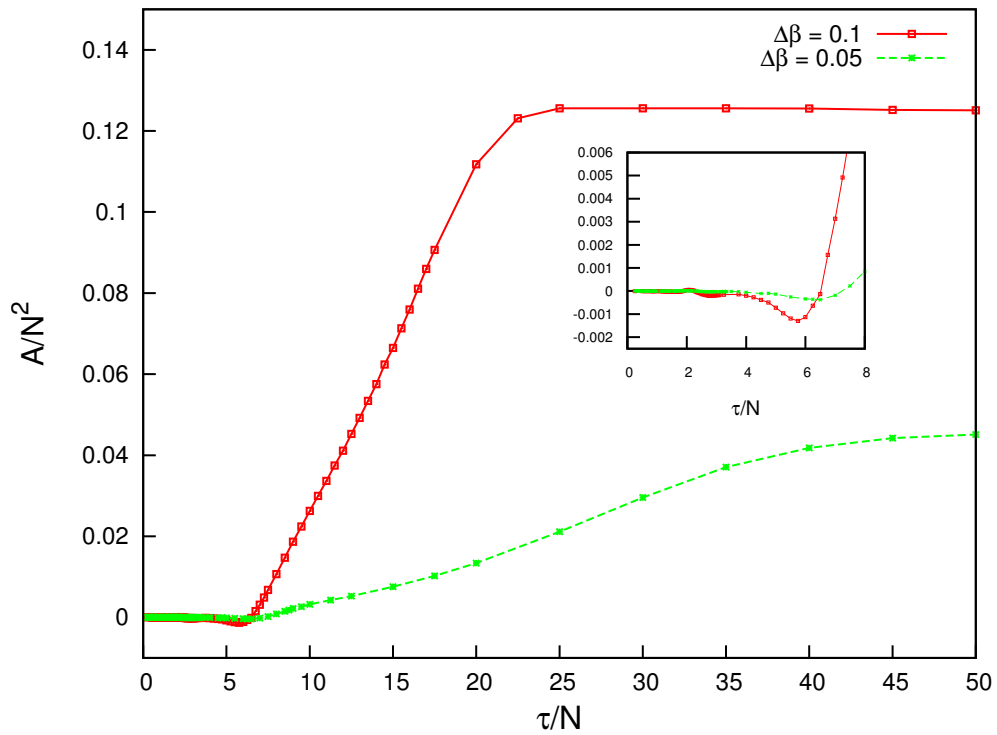


Figure 4.16: Hysteresis area for two different perturbation magnitudes, $\Delta\beta = 0.05$ and $\Delta\beta = 0.1$ and $N = 200$. The inset shows close up to the phase transition point.

4.2.3 Pulse Response

To be able to isolate the underlying mechanisms behind the different type of responses we have also carried out computations where we apply a pulse type of perturbation to the exit rate of first class of particles only. This pulse lasts one tenth of a period of $\tau = 10000$. The size of the pulse is $\beta_1 = 0.535$ and $t = 0.01\tau$ is its duration. When the duration ends the system relaxes to the nearest time-independent steady state. As a result, time-dependent shock profiles and average lattice occupation are obtained. To our surprise, both of them show significant oscillatory behavior.

Figure 4.17 displays the probability of particles on one wing of the hysteresis curve

$$P(n_1, t) = K \sum_{n_2=0}^{n_2=n_1-1} p(n_1, n_2, t).$$

Here K is a normalization constant. It is apparent that for smaller and larger values of n probability subsided earlier. Moreover, in figures 4.18 and 4.19 we show the behavior of shock profiles for various different times elapsed after the pulse ends. In short times after the pulse ends, since some particles leave during the pulse, large n_1 shocks are deformed into small n_1 shocks. Small n_1 shocks are lost completely since when the particle number in the lattice is that small its entire population is evacuated during the pulse. System recovers from these losses differently. Large n_1 shocks are restored exponentially and small n_1 shocks are recovered resulting in oscillatory damping.

We define a parameter of relaxation to the steady state after the pulse has been applied to the system. This was defined as the probability density deviation from that of the steady state:

$$\delta_1(t) = \sum_{n_1} [P(n_1, t) - P(n_1, \infty)]^2. \quad (4.10)$$

This parameter distinguishes the deformation of large n_1 shocks and the loss of small n_1 shocks. Fig. 4.20 shows deviation values for profiles corresponding to $n_1 < N/2$ and $n_1 > N/2$. The inset shows deviations for all values of n_1 . It is

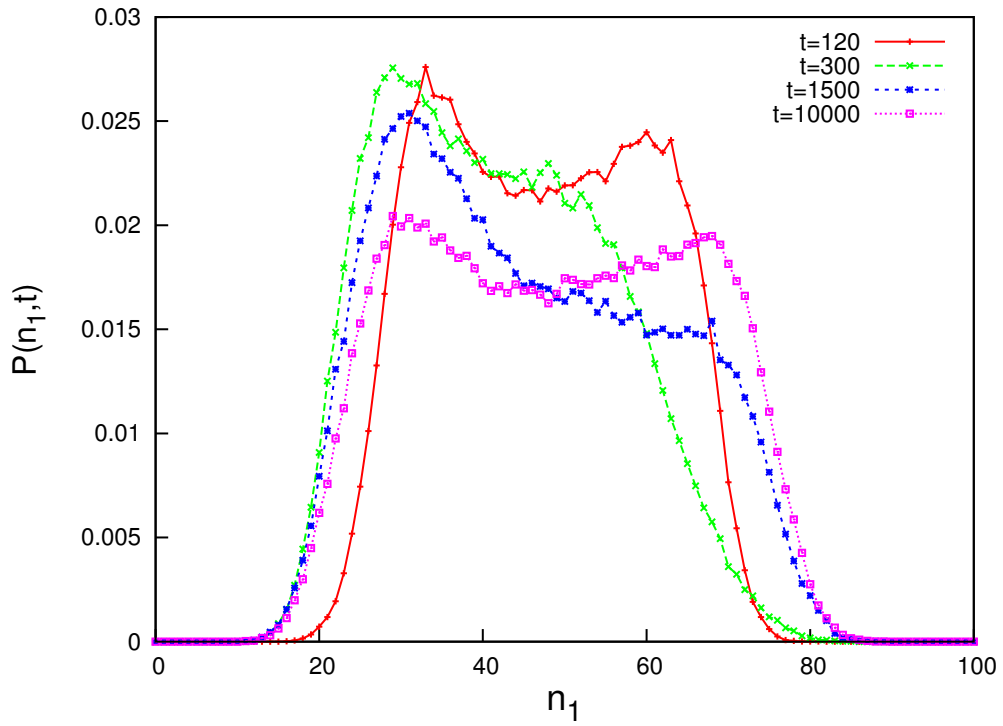


Figure 4.17: $P(n_1, t)$ for various values of t . $P(n_1, 10000)$ is a near steady-state distribution.

apparent that for both types of shocks deviation continues to increase after the pulse has ended. Eventually, the deviations relax to steady state values. It is seen that small n_1 distributions relax with shorter time-scale oscillations. This hints that, rather than the bulk effects the boundary rates are dominant in this relaxation. This surprising forms of behavior are the reasons behind the different types of response we report.

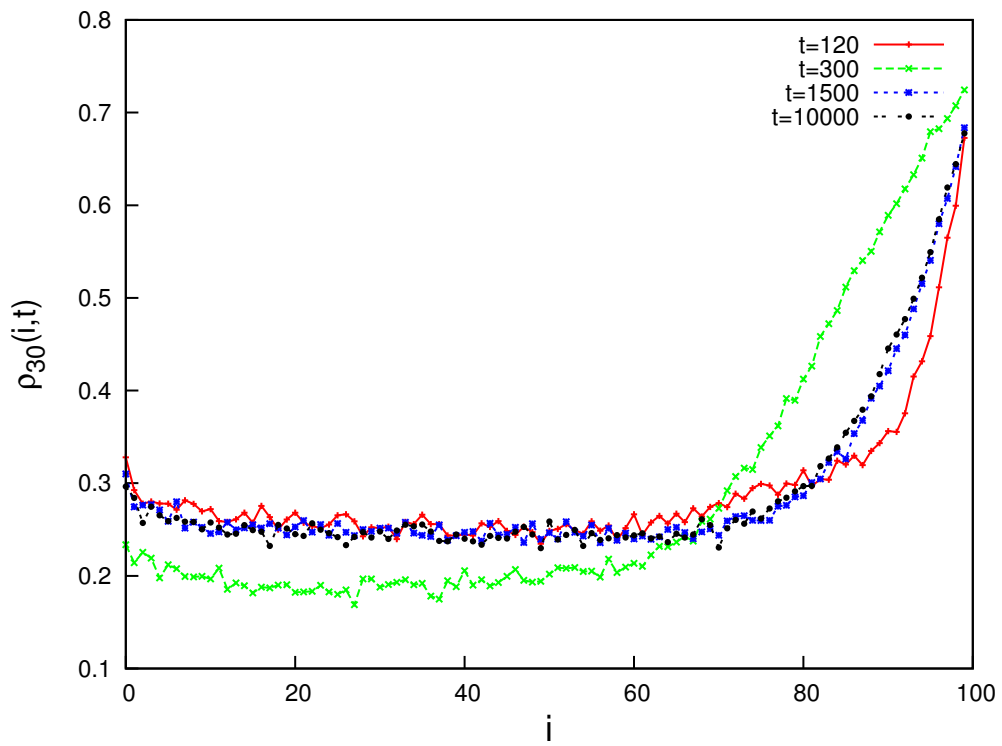


Figure 4.18: Shock densities corresponding to $n_1 = 30$ for various values of t .

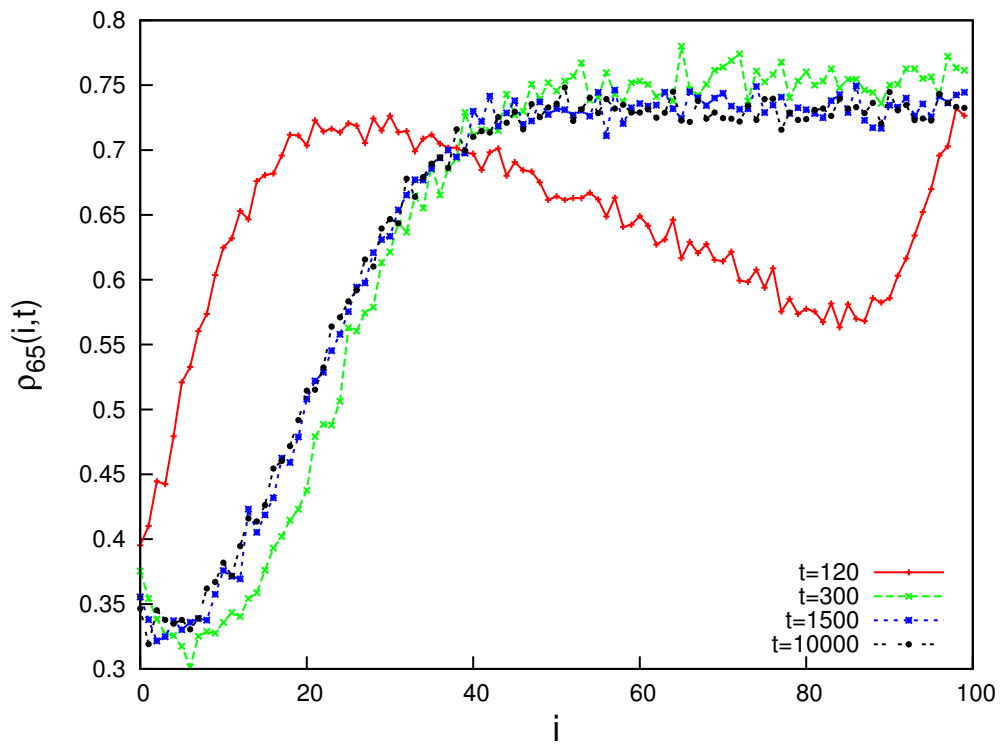


Figure 4.19: Shock profiles that are associated to particle number $n_1 = 65$ for various times t elapsed after the pulse.

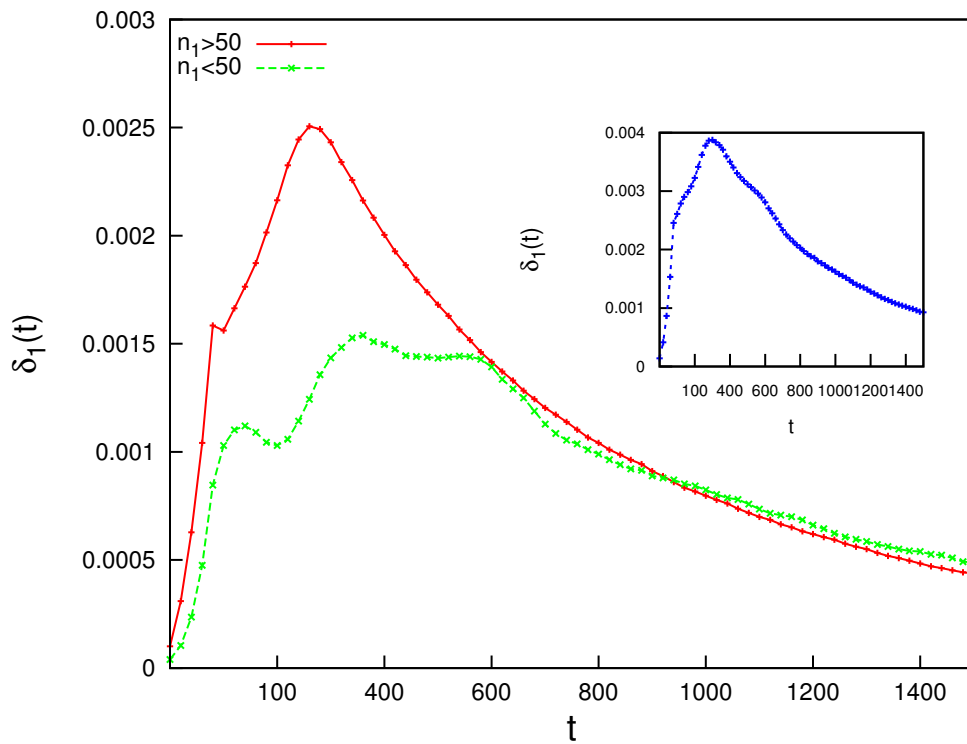


Figure 4.20: Relaxation of the deviation $\delta_1(t)$ for smaller and larger values of n_1 for $N = 100$. Inset shows $\delta_1(t)$ for all values of n_1 .

Chapter 5

Conclusions

We have reported the effect of sinusoidally oscillating boundary conditions (BC) on two different TASEP systems. The result of the boundary conditions is to generate an effective force on the Brownian motion of the shock profile. We report interesting phenomena of resonant nature arising due to the interference between this effective force and the system size.

In our first work, we have studied TASEP with single class of particles. We have demonstrated that under the oscillatory boundary conditions the motion of shock profile can be modeled with an over-damped Fokker-Planck system. Monte Carlo analysis of the former and the numerical analysis of the latter confirm that their results have a strongly frequency dependent nature and are qualitatively very similar. The phenomena can be explained by the matching of the particle number oscillations with the system size. Other forms of oscillations could be tried to strengthen interrelationship of the TASEP system with the FP analysis.

In our second work, we reported the results of a Monte Carlo study of TASEP with two classes of particles under oscillatory boundary conditions. We find that the response of the system again has strong frequency dependence. We track the response through the shape of the joint probability density: it extends or gets compact in response to changes in frequency. Variation of the size has

significant structure that does not depend on the magnitude of the drive, and scales with the system size. Basis of this phenomena is the motion of shock profiles within the system. Moreover, we reported the abrupt appearance of hysteresis as the frequency of perturbation is lowered. This abrupt appearance signals a dynamical phase transition. Appearance of hysteresis indicates that there is a velocity threshold in the system. Below it, the system flows between two states, each of which corresponds to the extreme limits of the BC, throughout an oscillation cycle. The characteristic velocity value is ~ 0.2 lattice sites per unit time. We identify near symmetric states in which the joint probability density preserves its form but is slightly displaced during a cycle. These effects appear at higher frequencies and the particular shape depends on the frequency.

In both of the works we report the response of the systems at the phase transition points, where systems support the motion of the shock profiles to the largest extent. Other points on the phase diagram, may also be analyzed to describe more dynamical mechanisms.

Bibliography

- [1] P. Bak and M. Paczuski, “Complexity, contingency, and criticality,” *Proceedings of the National Academy of Sciences*, vol. 92, no. 15, pp. 6689–6696, 1995.
- [2] T. Chou, K. Mallick, and R. K. P. Zia, “Non-equilibrium statistical mechanics: from a paradigmatic model to biological transport,” *Reports on Progress in Physics*, vol. 74, no. 11, p. 116601, 2011.
- [3] J. W. Gibbs, “On the equilibrium of heterogeneous substances,” *American Journal of Science*, no. 96, pp. 441–458, 1878.
- [4] K. Huang, *Introduction to statistical physics*. Taylor Francis, 2001.
- [5] L. E. Reichl and I. Prigogine, *A Modern Course in Statistical Physics*. University of Texas Press Austin, 1980, vol. 71.
- [6] R. Pathria, *Statistical Mechanics*. Elsevier, 1972.
- [7] M. Plischke and B. Bergersen, *Equilibrium Statistical Physics*. World Scientific, 2006.
- [8] K. G. Wilson, “The renormalization group: Critical phenomena and the kondo problem,” *Reviews of Modern Physics*, vol. 47, no. 4, p. 773, 1975.
- [9] J. Thijssen, *Computational physics*. Cambridge university press, 2007.
- [10] R. Kubo, “The fluctuation-dissipation theorem,” *Reports on progress in physics*, vol. 29, no. 1, p. 255, 1966.

- [11] L. Leuzzi and T. M. Nieuwenhuizen, *Thermodynamics of the glassy state*. CRC Press, 2007.
- [12] M. Henkel, H. Hinrichsen, S. Lübeck, and M. Pleimling, *Non-equilibrium phase transitions*. Springer, 2008, vol. 1.
- [13] J.-P. Bouchaud, L. F. Cugliandolo, J. Kurchan, and M. Mezard, “Out of equilibrium dynamics in spin-glasses and other glassy systems,” *Spin glasses and random fields*, pp. 161–223, 1998.
- [14] Z. Rácz, “Nonequilibrium phase transitions,” *arXiv preprint cond-mat/0210435*, 2002.
- [15] Y.-q. Ma and J.-w. Liu, “The competing glauher and kawasaki dynamics induced phase transition in the ferromagnetic ising model,” *Physics Letters A*, vol. 238, no. 2, pp. 159–163, 1998.
- [16] T. Per Bak and K. Wiesenfeld, “Self-organized criticality: and explanation of 1/f noise,” *Phys. Rev. Lett*, vol. 59, pp. 381–384, 1987.
- [17] M. Cross and H. Greenside, *Pattern formation and dynamics in nonequilibrium systems*. Cambridge University Press, 2009.
- [18] J. P. Gollub and J. Langer, “Pattern formation in nonequilibrium physics,” *Reviews of Modern Physics*, vol. 71, no. 2, p. S396, 1999.
- [19] C. T. MacDonald, J. H. Gibbs, and A. C. Pipkin, “Kinetics of biopolymerization on nucleic acid templates,” *Biopolymers*, vol. 6, no. 1, pp. 1–25, 1968.
- [20] C. T. MacDonald and J. H. Gibbs, “Concerning the kinetics of polypeptide synthesis on polyribosomes,” *Biopolymers*, vol. 7, no. 5, pp. 707–725, 1969.
- [21] F. Spitzer, “Interaction of markov processes,” *Advances in Mathematics*, vol. 5, no. 2, pp. 246 – 290, 1970.
- [22] N. Rajewsky, L. Santen, A. Schadschneider, and M. Schreckenberg, “The asymmetric exclusion process: Comparison of update procedures,” *Journal of statistical physics*, vol. 92, no. 1-2, pp. 151–194, 1998.

- [23] A. Rákos and G. M. Schütz, “Bethe ansatz and current distribution for the tasep with particle-dependent hopping rates,” *arXiv preprint cond-mat/0506525*, 2005.
- [24] M. Evans, R. Juhasz, and L. Santen, “Shock formation in an exclusion process with creation and annihilation,” *Physical Review E*, vol. 68, no. 2, p. 026117, 2003.
- [25] K. Krebs, F. Jafarpour, and G. Schütz, “Microscopic structure of travelling wave solutions in a class of stochastic interacting particle systems,” *New Journal of Physics*, vol. 5, no. 1, p. 145, 2003.
- [26] V. Karimipour, “Multispecies asymmetric simple exclusion process and its relation to traffic flow,” *Physical Review E*, vol. 59, no. 1, p. 205, 1999.
- [27] R. Jiang, M.-B. Hu, B. Jia, R. Wang, and Q.-S. Wu, “Spontaneous symmetry breaking and periodic structure in a multilane system,” *Physical Review E*, vol. 76, no. 3, p. 036116, 2007.
- [28] S. Katz, J. L. Lebowitz, and H. Spohn, “Phase transitions in stationary nonequilibrium states of model lattice systems,” *Physical Review B*, vol. 28, no. 3, p. 1655, 1983.
- [29] S. Katz, J. L. Lebowitz, and H. Spohn, “Nonequilibrium steady states of stochastic lattice gas models of fast ionic conductors,” *Journal of statistical physics*, vol. 34, no. 3-4, pp. 497–537, 1984.
- [30] R. Zia, “Twenty five years after kls: A celebration of non-equilibrium statistical mechanics,” *Journal of Statistical Physics*, vol. 138, no. 1-3, pp. 20–28, 2010.
- [31] I. Corwin, “The kardar–parisi–zhang equation and universality class,” *Random matrices: Theory and applications*, vol. 1, no. 01, p. 1130001, 2012.
- [32] A. Schadschneider, D. Chowdhury, and K. Nishinari, *Stochastic transport in complex systems: from molecules to vehicles*. Elsevier, 2010.

- [33] M. R. Evans and T. Hanney, “Nonequilibrium statistical mechanics of the zero-range process and related models,” *Journal of Physics A: Mathematical and General*, vol. 38, no. 19, p. R195, 2005.
- [34] B. Derrida and K. Mallick, “Exact diffusion constant for the one-dimensional partially asymmetric exclusion model,” *Journal of Physics A: Mathematical and General*, vol. 30, no. 4, p. 1031, 1997.
- [35] A. Benassi and J.-P. Fouque, “Hydrodynamical limit for the asymmetric simple exclusion process,” *The Annals of Probability*, pp. 546–560, 1987.
- [36] G. Schütz, C. Domb, and J. Lebowitz, “Phase transitions and critical phenomena,” 2001.
- [37] M. Kardar, G. Parisi, and Y.-C. Zhang, “Dynamic scaling of growing interfaces,” *Physical Review Letters*, vol. 56, no. 9, p. 889, 1986.
- [38] O. Golinelli and K. Mallick, “The asymmetric simple exclusion process: an integrable model for non-equilibrium statistical mechanics,” *Journal of Physics A: Mathematical and General*, vol. 39, no. 41, p. 12679, 2006.
- [39] B. Derrida, S. A. Janowsky, J. L. Lebowitz, and E. R. Speer, “Exact solution of the totally asymmetric simple exclusion process: shock profiles,” *Journal of statistical physics*, vol. 73, no. 5-6, pp. 813–842, 1993.
- [40] L. Faddeev, “Integrable models in 1+ 1 dimensional quantum field theory,” CEA Centre d’Etudes Nucleaires de Saclay, Tech. Rep., 1982.
- [41] B. Derrida, J. Lebowitz, and E. Speer, “Exact large deviation functional of a stationary open driven diffusive system: the asymmetric exclusion process,” *Journal of statistical physics*, vol. 110, no. 3-6, pp. 775–810, 2003.
- [42] E. Speer, “The two species totally asymmetric exclusion process micro, meso and macroscopic approaches in physics ((nato workshop on three levels, leuven)) ed m fannes, c maes and a verbeure,” *C Maes and A Verbeure*, 1993.
- [43] D. Dhar, “An exactly solved model for interfacial growth,” *Phase transitions*, vol. 9, no. 1, p. 51, 1987.

- [44] L.-H. Gwa and H. Spohn, “Bethe solution for the dynamical-scaling exponent of the noisy burgers equation,” *Physical Review A*, vol. 46, no. 2, p. 844, 1992.
- [45] D. Kim, “Bethe ansatz solution for crossover scaling functions of the asymmetric xxz chain and the kardar-parisi-zhang-type growth model,” *Physical Review E*, vol. 52, no. 4, p. 3512, 1995.
- [46] O. Golinelli and K. Mallick, “Bethe ansatz calculation of the spectral gap of the asymmetric exclusion process,” *Journal of Physics A: Mathematical and General*, vol. 37, no. 10, p. 3321, 2004.
- [47] O. Golinelli and K. Mallick, “Spectral gap of the totally asymmetric exclusion process at arbitrary filling,” *Journal of Physics A: Mathematical and General*, vol. 38, no. 7, p. 1419, 2005.
- [48] B. Derrida and J. L. Lebowitz, “Exact large deviation function in the asymmetric exclusion process,” *Physical review letters*, vol. 80, no. 2, p. 209, 1998.
- [49] B. Derrida and C. Appert, “Universal large-deviation function of the kardar–parisi–zhang equation in one dimension,” *Journal of statistical physics*, vol. 94, no. 1-2, pp. 1–30, 1999.
- [50] B. Derrida and M. Evans, “Bethe ansatz solution for a defect particle in the asymmetric exclusion process,” *Journal of Physics A: Mathematical and General*, vol. 32, no. 26, p. 4833, 1999.
- [51] K. Mallick and S. Sandow, “Finite-dimensional representations of the quadratic algebra: applications to the exclusion process,” *Journal of Physics A: Mathematical and General*, vol. 30, no. 13, p. 4513, 1997.
- [52] T. Nagao, M. Katori, and H. Tanemura, “Dynamical correlations among vicious random walkers,” *Physics Letters A*, vol. 307, no. 1, pp. 29–35, 2003.
- [53] S. Corteel, L. K. Williams *et al.*, “Tableaux combinatorics for the asymmetric exclusion process and askey-wilson polynomials,” *Duke Mathematical Journal*, vol. 159, no. 3, pp. 385–415, 2011.

- [54] T. Sasamoto, “One-dimensional partially asymmetric simple exclusion process with open boundaries: orthogonal polynomials approach,” *Journal of Physics A: Mathematical and General*, vol. 32, no. 41, p. 7109, 1999.
- [55] T. Nagao and T. Sasamoto, “Asymmetric simple exclusion process and modified random matrix ensembles,” *Nuclear Physics B*, vol. 699, no. 3, pp. 487–502, 2004.
- [56] C. A. Tracy and H. Widom, “A fredholm determinant representation in asep,” *Journal of Statistical Physics*, vol. 132, no. 2, pp. 291–300, 2008.
- [57] C. T. MacDonald, J. H. Gibbs, and A. C. Pipkin, “Kinetics of biopolymerization on nucleic acid templates,” *Biopolymers*, vol. 6, no. 1, pp. 1–25, 1968.
- [58] K. Sugden, M. Evans, W. Poon, and N. Read, “Model of hyphal tip growth involving microtubule-based transport,” *Physical Review E*, vol. 75, no. 3, p. 031909, 2007.
- [59] M. Evans and S. K. E. P, “An exclusion process for modelling fungal hyphal growth,” *Physica A*, vol. 384, no. 53, 2007.
- [60] A. Gabel, P. Krapivsky, and S. Redner, “Facilitated asymmetric exclusion,” *Physical review letters*, vol. 105, no. 21, p. 210603, 2010.
- [61] P. M. Richards, “Theory of one-dimensional hopping conductivity and diffusion,” *Physical Review B*, vol. 16, no. 4, p. 1393, 1977.
- [62] D. G. Levitt, “Dynamics of a single-file pore: non-fickian behavior,” *Physical Review A*, vol. 8, no. 6, p. 3050, 1973.
- [63] B. Widom, J. Viovy, and A. Defontaine, “Repton model of gel electrophoresis and diffusion,” *Journal de Physique I*, vol. 1, no. 12, pp. 1759–1784, 1991.
- [64] D. Wolf, M. Schreckenberg, and A. Bachem, “Traffic and granular flow,” 1996.

- [65] T. Halpin-Healy and Y.-C. Zhang, “Kinetic roughening phenomena, stochastic growth, directed polymers and all that. aspects of multidisciplinary statistical mechanics,” *Physics reports*, vol. 254, no. 4, pp. 215–414, 1995.
- [66] J. Krug, “Origins of scale invariance in growth processes,” *Advances in Physics*, vol. 46, no. 2, pp. 139–282, 1997.
- [67] R. Bundschuh, “Asymmetric exclusion process and extremal statistics of random sequences,” *Physical Review E*, vol. 65, no. 3, p. 031911, 2002.
- [68] D. Yanagisawa, A. Tomoeda, R. Jiang, and K. Nishinari, “Excluded volume effect in queueing theory,” *JSIAM Letters*, vol. 2, no. 0, pp. 61–64, 2010.
- [69] I. Neri, N. Kern, and A. Parmeggiani, “Totally asymmetric simple exclusion process on networks,” *Physical review letters*, vol. 107, no. 6, p. 068702, 2011.
- [70] G. M. Schütz, “Critical phenomena and universal dynamics in one-dimensional driven diffusive systems with two species of particles,” *Journal of Physics A: Mathematical and General*, vol. 36, no. 36, p. R339, 2003.
- [71] J. Krug, “Boundary-induced phase transitions in driven diffusive systems,” *Physical review letters*, vol. 67, no. 14, p. 1882, 1991.
- [72] P. Ferrari, C. Kipnis, E. Saada *et al.*, “Microscopic structure of travelling waves in the asymmetric simple exclusion process,” *The Annals of Probability*, vol. 19, no. 1, pp. 226–244, 1991.
- [73] A. De Masi, C. Kipnis, E. Presutti, and E. Saada, “Microscopic structure at the shock in the asymmetric simple exclusion,” *Stochastics: An International Journal of Probability and Stochastic Processes*, vol. 27, no. 3, pp. 151–165, 1989.
- [74] P. A. Ferrari, “Shock fluctuations in asymmetric simple exclusion,” *Probability theory and related fields*, vol. 91, no. 1, pp. 81–101, 1992.

- [75] J. L. Lebowitz, E. Presutti, and H. Spohn, “Microscopic models of hydrodynamic behavior,” *Journal of Statistical Physics*, vol. 51, no. 5-6, pp. 841–862, 1988.
- [76] G. Schütz, “Time-dependent correlation functions in a one-dimensional asymmetric exclusion process,” *Physical Review E*, vol. 47, no. 6, p. 4265, 1993.
- [77] M. R. Evans, D. P. Foster, C. Godrèche, and D. Mukamel, “Spontaneous symmetry breaking in a one dimensional driven diffusive system,” *Physical review letters*, vol. 74, no. 2, p. 208, 1995.
- [78] A. B. Kolomeisky, G. M. Schütz, E. B. Kolomeisky, and J. P. Straley, “Phase diagram of one-dimensional driven lattice gases with open boundaries,” *Journal of Physics A: Mathematical and General*, vol. 31, no. 33, p. 6911, 1998.
- [79] D. W. Erickson, G. Pruessner, B. Schmittmann, and R. Zia, “Spurious phase in a model for traffic on a bridge,” *Journal of Physics A: Mathematical and General*, vol. 38, no. 41, p. L659, 2005.
- [80] P. F. Arndt, T. Heinzl, and V. Rittenberg, “First-order phase transitions in one-dimensional steady states,” *Journal of statistical physics*, vol. 90, no. 3-4, pp. 783–815, 1998.
- [81] M. Clincy, M. Evans, and D. Mukamel, “Symmetry breaking through a sequence of transitions in a driven diffusive system,” *Journal of Physics A: Mathematical and General*, vol. 34, no. 47, p. 9923, 2001.
- [82] W. R. Gilks, *Markov chain monte carlo*. Wiley Online Library, 2005.
- [83] P. H. Acioli, “Review of quantum monte carlo methods and their applications,” *Journal of Molecular Structure: THEOCHEM*, vol. 394, no. 2, pp. 75–85, 1997.
- [84] F. James, “Monte carlo theory and practice,” *Reports on Progress in Physics*, vol. 43, no. 9, p. 1145, 1980.

- [85] N. Metropolis and S. Ulam, “The monte carlo method,” *Journal of the American statistical association*, vol. 44, no. 247, pp. 335–341, 1949.
- [86] N. Rajewsky, L. Santen, A. Schadschneider, and M. Schreckenberg, “The asymmetric exclusion process: Comparison of update procedures,” *Journal of statistical physics*, vol. 92, no. 1-2, pp. 151–194, 1998.
- [87] A. D. Fokker, “Die mittlere energie rotierender elektrischer dipole im strahlungsfeld,” *Annalen der Physik*, vol. 348, no. 5, pp. 810–820, 1914.
- [88] M. Planck, “Über einen Satz der statistischen Dynamik and seine Erweiterung in der Quantentheorie,” *Sitzungsberichte der Preussischen Akademie der Wissenschaften*, vol. 24, pp. 324–341, 1917.
- [89] A. Kolmogoroff, “Über die analytischen methoden in der wahrscheinlichkeitsrechnung,” *Mathematische Annalen*, vol. 104, no. 1, pp. 415–458, 1931.
- [90] H. Risken, “The fokker-planck equation, volume 18 of springer series in synergetics,” 1989.
- [91] P. Hänggi and H. Thomas, “Stochastic processes: Time evolution, symmetries and linear response,” *Physics Reports*, vol. 88, no. 4, pp. 207–319, 1982.
- [92] R. Bartussek, P. Hänggi, and J. G. Kissner, “Periodically rocked thermal ratchets,” *EPL (Europhysics Letters)*, vol. 28, no. 7, p. 459, 1994.
- [93] P. Landa and P. V. McClintock, “Vibrational resonance,” *Journal of Physics A: Mathematical and general*, vol. 33, no. 45, p. L433, 2000.
- [94] D. Cubero, J. Casado-Pascual, and F. Renzoni, “Irrationality and quasiperiodicity in driven nonlinear systems,” *Physical review letters*, vol. 112, no. 17, p. 174102, 2014.
- [95] P. Hänggi and F. Marchesoni, “Artificial brownian motors: Controlling transport on the nanoscale,” *Reviews of Modern Physics*, vol. 81, no. 1, p. 387, 2009.

- [96] R. Benzi, A. Sutera, and A. Vulpiani, “The mechanism of stochastic resonance,” *Journal of Physics A: mathematical and general*, vol. 14, no. 11, p. L453, 1981.
- [97] P. Jung and P. Hänggi, “Stochastic nonlinear dynamics modulated by external periodic forces,” *EPL (Europhysics Letters)*, vol. 8, no. 6, p. 505, 1989.
- [98] L. Gammaitoni and F. Marchesoni, “Menichella-saetta . and santucci s,” *Phys. Rev. Lett*, vol. 62, p. 349, 1989.
- [99] P. Jung, “Periodically driven stochastic systems,” *Physics Reports*, vol. 234, no. 4, pp. 175–295, 1993.
- [100] F. Moss, “Stochastic resonance: from the ice ages to the monkeys ear,” *Contemporary problems in statistical physics*, pp. 205–253, 1994.
- [101] L. Gammaitoni, P. Hänggi, P. Jung, and F. Marchesoni, “Stochastic resonance,” *Reviews of modern physics*, vol. 70, no. 1, p. 223, 1998.
- [102] B. Spagnolo, D. Valenti, and A. Fiasconaro, “Noise in ecosystems: a short review,” *arXiv preprint q-bio/0403004*, 2004.
- [103] J.-C. Li, C. Li, and D.-C. Mei, “Effects of time delay on stochastic resonance of the stock prices in financial system,” *Physics Letters A*, vol. 378, no. 30, pp. 1997–2000, 2014.
- [104] Y. V. Ushakov, A. Dubkov, and B. Spagnolo, “Regularity of spike trains and harmony perception in a model of the auditory system,” *Physical review letters*, vol. 107, no. 10, p. 108103, 2011.
- [105] S. Martignoli, F. Gomez, and R. Stoop, “Pitch sensation involves stochastic resonance,” *Scientific reports*, vol. 3, 2013.
- [106] N. Zygouras, “Exponential convergence for a periodically driven semilinear heat equation,” in *Annales de l’Institut Henri Poincaré (C) Non Linear Analysis*, vol. 26, no. 1. Elsevier, 2009, pp. 271–284.

- [107] A. Shit, S. Chattopadhyay, and J. R. Chaudhuri, “Kapitza-landau time window for a periodically driven system with friction: a system-bath hamiltonian approach,” *The European Physical Journal B*, vol. 86, no. 1, pp. 1–9, 2013.
- [108] V. Popkov, M. Salerno, and G. M. Schütz, “Asymmetric simple exclusion process with periodic boundary driving,” *Physical Review E*, vol. 78, no. 1, p. 011122, 2008.
- [109] U. Basu, D. Chaudhuri, and P. Mohanty, “Bimodal response in periodically driven diffusive systems,” *Physical Review E*, vol. 83, no. 3, p. 031115, 2011.
- [110] A. Rákos, M. Paessens, and G. Schütz, “Hysteresis in one-dimensional reaction-diffusion systems,” *Physical review letters*, vol. 91, no. 23, p. 238302, 2003.